Thesis

Analysis of Cavernous Sinus Compartments in Relation to Pituitary Adenoma Extension

submitted by

Paul Greiner

in partial fulfilment of the requirements for the degree of

Doktor(in) der gesamten Heilkunde

(Dr.$^{(in)}$ med. univ.)

at the

Medical University of Graz

executed at the

University Department of Neurosurgery

under the supervision of

Ass.-Prof. Priv.-Doz. Dr.med.univ. Dr.scient.med. Alexander Micko

Graz, 03.04.2025

Statement of Originality

I hereby confirm that the present diploma thesis is the result of my own independent scholarly work. I also confirm that in all cases, where material from the work of others (in books, articles, essays, dissertations, and on the internet) is acknowledged, quotations and paraphrases are clearly indicated. No material other than that cited in the reference list has been used. I have read and understood the Medical University's regulations and procedures concerning plagiarism.
Furthermore, I hereby declare that if artificial intelligence (AI) tools were used for the generation and/or correction of certain text passages in the creation of this work, such employment was conducted in compliance with ethical principles, academic integrity, and the regulations of my university. Additionally, it was ensured that this usage was transparently disclosed and appropriately attributed.

Graz, 03.04.2025 Paul Greiner m.p.

Zusammenfassung

Hintergrund

Hypophysenadenome sind in der Lage, benachbarte Strukturen wie Knochen, Dura mater oder die Keilbeinhöhle zu infiltrieren (1,2). Das Ausmaß der Invasion in den parasellären Raum, insbesondere in den Sinus cavernosus, ist ein wichtiges prognostisches Element sowohl für das chirurgische Ergebnis als auch für das Wiederauftreten (1,2). Es sollte jedoch zwischen einer echten Invasion, daher einem infiltrativen Wachstum in den Sinus cavernosus, und einer bloßen Verlagerung parasellärer Strukturen aufgrund der Tumormasse unterschieden werden (1). Ziel der Diplomarbeit war es, eine statistische Korrelation zwischen der Invasion von Hypophysenadenomen in die Kompartimente des Sinus cavernosus und morphologischen Merkmalen nachzuweisen.

Methoden

Diese retrospektive Analyse von Patientinnen- und Patientendaten umfasste 273 Patientinnen und Patienten, die sich zwischen 2013 und 2022 an der Universitätsklinik für Neurochirurgie der Medizinischen Universität Graz einer endoskopischen transnasalen transsphenoidalen Operation wegen eines Hypophysenadenoms unterzogen haben. Es wurden zwei Studiengruppen definiert, basierend auf der Entscheidung, ob der Tumor Anzeichen einer Invasivität in den Sinus cavernosus aufwies (Gruppe: Invasion, Inv) oder nicht (Gruppe: Nicht-invasiv, Non-Inv). In 8 Fällen lag kein Operationsbericht vor, sodass 265 Patientinnen und Patienten für die weitere Analyse in dieser Studie berücksichtigt wurden.

Ergebnisse

In der Gruppe Non-Inv wurde in 165 Fällen (62,3 %) keine endoskopisch beobachtete Invasion in den Sinus cavernosus festgestellt, während in 100 Fällen (37,7 %) eindeutige Anzeichen einer Invasion (Gruppe: Inv) festgestellt wurden. Die mediane Größe der Hypophysenadenome betrug in der Gruppe Non-Inv 20,3 mm (IQR: 14,9–27,5) und in der Gruppe Inv 29 mm (IQR: 20–38,4, p = < 0,001). Das mittlere Volumen betrug 2,5 cm^3 (IQR: 1,2–6,7) in der Gruppe Non-Inv und 7,3 cm^3 (IQR: 2,8–13,3) in der Gruppe Inv (p = < 0,001).

Die überarbeitete Knosp-Einstufung in der Gruppe Non-Inv zeigte: Grad 0: 62 (37,6 %), Grad 1: 38 (23 %), Grad 2: 32 (19,4 %), Grad 3A: 25 (15,2 %), Grad 3B: 4 (2,4

%) und Grad 4: 4 (2,4 %). In der Gruppe Inv: Grad 0: 23 (23 %), Grad 1: 17 (17 %), Grad 2: 14 (14 %), Grad 3A: 22 (22 %), Grad 3B: 5 (5 %) und Grad 4: 19 (19 %); (p = < 0,001). Insbesondere Hypophysenadenome Grad 4 wurden in der Gruppe Inv (19 %) signifikant häufiger gefunden als in der Gruppe Non-Inv (2,4 %, p = < 0,001). Das binomiale Regressionsmodell für Makroadenome zeigte, dass Adenome mit einem Volumen von über 1 cm³ (OR: 4,627, 95 % KI: 1,476–14,498, p = 0,009) unabhängig mit einer Invasion in den Sinus cavernosus assoziiert sind. Darüber hinaus konnte festgestellt werden, dass die Odds Ratio (3,275, 95 % KI: 1,649–6,503) für Makroadenome mit faseriger Konsistenz signifikant höher (p = < 0,001) ist als für Adenome mit einer weichen Konsistenz.

Die binomiale Regression für nicht funktionelle Adenome zeigte, dass Adenome mit einem Volumen von über 1,6 cm^3 (OR: 4,091, 95 %: KI 1,310–12,778, p = 0,015) unabhängig mit einer Invasion in den Sinus cavernosus assoziiert sind. Außerdem ist die Odds Ratio (2,710, 95 % KI: 1,250–5,875) für eine Invasion in den Sinus cavernosus bei faserigen, nicht funktionellen Adenomen signifikant höher (p = 0,012) als bei Adenomen mit weicher Konsistenz.

Conclusio

Es wurde eine Korrelation zwischen der Größe, dem Volumen und der Konsistenz des Adenoms und seiner Invasion in den Sinus cavernosus nachgewiesen. Dabei zeigte sich eine starke unabhängige Assoziation zwischen der faserigen Konsistenz der Hypophysenadenome und der Invasivität in den Sinus cavernosus. Darüber hinaus wurde bei nicht funktionellen Hypophysenadenomen ein Volumen > 1,6 cm³ als unabhängiger Faktor gefunden, der mit einer Invasion in den Sinus cavernosus assoziiert ist.

Die Ergebnisse dieser Arbeit deuten darauf hin, dass spezifische präoperative Parameter die Invasivität eines Hypophysenadenoms vorhersagen können. Diese Faktoren können eine bessere Patientinnen- und Patientenberatung ermöglichen und zur Entwicklung einer multimodalen Behandlungsstrategie beitragen, die chirurgische Eingriffe, medikamentöse Therapien und radiochirurgische Verfahren umfasst.

Abstract

Background

Pituitary adenomas are capable of infiltrating adjacent structures such as bone, dura mater or the sphenoid sinus (1,2). The degree of invasion into the parasellar space, particularly into the cavernous sinus, is a significant prognostic element for both surgical outcome and recurrence (1,2). However, a distinction should be made between true invasion, e.g. infiltrative growth into the cavernous sinus or solely a displacement of parasellar structures due to tumor mass (1). The aim of the diploma thesis was to demonstrate a statistical correlation between invasion of pituitary adenomas into the compartments of the cavernous sinus and morphological characteristics.

Methods

This retrospective analysis of patient data included 273 patients who underwent endoscopic transnasal transsphenoidal surgery for pituitary adenoma between 2013 and 2022 at the Department of Neurosurgery, Medical University of Graz. Two study groups were defined based on the decision if the tumor showed signs of invasiveness into the cavernous sinus (Group: Invasion, Inv) or not (Group: Non-Invasive, Non-Inv). In 8 cases, no operation report was available and therefore 265 patients were included for further analysis in this study.

Results

In group Non-Inv, no endoscopically observed invasion into the cavernous sinus was detected in 165 cases (62.3%), whereas clear signs of invasion (Group: Inv) were found in 100 cases (37.7%). The median size of pituitary adenomas in group Non-Inv was 20.3 mm (IQR: 14.9–27.5), in group Inv 29 mm (IQR: 20–38.4, p = < 0.001). The median volume was 2.5 cm^3 (IQR: 1.2–6.7) in group Non-Inv and 7.3 cm^3 (IQR: 2.8–13.3) in group Inv (p = < 0.001).

The revised Knosp Grading in group Non-Inv showed: Grade 0: 62 (37.6%), Grade 1: 38 (23%), Grade 2: 32 (19.4%), Grade 3A: 25 (15.2%), Grade 3B: 4 (2.4%) and Grade 4: 4 (2.4%). In group Inv: Grade 0: 23 (23%), Grade 1: 17 (17%), Grade 2: 14 (14 %), Grade 3A: 22 (22%), Grade 3B: 5 (5%) and Grade 4: 19 (19%); (p = < 0.001). Particularly Grade 4 pituitary adenomas were found significantly more often in group Inv (19%) than in group Non-Inv (2.4%, p = < 0.001).

The binomial regression model for macroadenomas showed that adenomas which have a volume above 1 cm^3 (OR: 4.627, 95% CI: 1.476–14.498, p = 0.009) are independently associated with invasion into the cavernous sinus. In addition, it can be established that the odds ratio (3.275, 95% CI: 1.649–6.503) for macroadenomas with a fibrous consistency is significantly (p = < 0.001) higher as for adenomas with a soft consistency.

The binomial regression for non-functioning adenomas showed that adenomas which have a volume above 1.6 cm^3 (OR: 4.091, 95%: CI 1.310–12.778, p = 0.015) are independently associated with invasion into the cavernous sinus. Furthermore, the odds ratio (2.710, 95% CI: 1.250–5.875) for invasion into the cavernous sinus for fibrous non-functioning adenomas is significantly higher (p = 0.012) as for adenomas with a soft consistency.

Conclusion

A correlation has been demonstrated between the size, volume, and consistency of the adenoma and its invasion into the cavernous sinus.

In particular, a fibrous consistency of the pituitary adenomas showed a strong independent association with invasiveness into the cavernous sinus. Furthermore, in non-functioning pituitary adenomas a volume > 1.6 cm^3 was found as an independent factor being associated with invasion into the cavernous sinus.

The findings of this thesis indicate that specific preoperative parameters can predict the invasiveness of a pituitary adenoma. These factors may facilitate improved patient counselling and contribute to the development of a multimodal treatment strategy, incorporating surgical intervention, medical therapy, and radiosurgery.

Publication

At the time of submission, this thesis had not been published.

Index

List of abbreviations

A.	Artery
ACTH	Adrenocorticotropic hormone
ADH	Antidiuretic hormone
ANT. GENU	Anterior genu
ANT. WALL	Anterior wall
CAV.	Cavernous
CISS	Constructive interference in steady state
CM^3	Cubic centimeters
CN	Cranial nerve
CS	Cavernous sinus
CT	Computed tomography
DIS.	Distal
DIST. RING	Distal dural ring
ER ALPHA	Estrogen receptor alpha
ET AL.	Et alia
FSH	Follicle-stimulating hormone
GH	Growth hormone
HISTO.	Histopathological
ICA	Internal carotid artery
IGF-1	Insulin-like growth factor 1
INF. COMP.	Inferior compartment
INF. LAT. TR.	Inferolateral trunk
INF. PETR. SIN.	Inferior petrosal sinus
INTERCLIN. LIG.	Interclinoidal ligament
INTERD.	Interdural
IQR	Interquartile range
INV	Invasion

LING. PROC.	Lingual process
MAX.	Maxillary
MEN-HYP. TRUNK	Meningohypophyseal trunk
MG	Milligram
MM	Millimeter
MPRAGE	Magnetization prepared rapid gradient echo
MRA	Magnetic resonance angiography
MRI	Magnetic resonance imaging
N.	Nerve
NON-FUNCTION.	Non-functioning
NON-INV	Non-invasive
OCULO-MOTOR TR.	Oculomotor triangle
OR	Odds ratio
PARACLIN.	Paraclinoidal
PCP	Posterior clinoidal process
PET. APEX	Petrosal apex
PETR. APEX	Petrous apex
PETRO-SPH. LIG.	Petro-sphenoidal ligament
PIT-1	Pituitary transcription factor 1
PIT.	Pituitary
POST. COMP.	Posterior compartment
POST. GENU	Posterior genu
PRL	Prolactin
PROX.	Proximal
PROX. RING	Proximal dural ring
PTERYGOSPHEN. FISS.	Pterygosphenoidal fissure
SF-1	Steroidogenic factor 1
SUP. COMP.	Superior compartment
SUP. PETR. SIN.	Superior petrosal sinus
SYMP.	Sympathetic

SYMP. N.	Sympathetic nerve
T3	Triiodothyronine
T4	Thyroxine
TOF	Time of flight
TPIT	T-box transcription factor
TSH	Thyroid-stimulating hormone
V1	Ophthalmic nerve
V2	Maxillary nerve
V3	Mandibular nerve
VIBE	Volumetric interpolated breath-hold examination
WHO	World Health Organization

List of figures

List of tables

1. Introduction

1.1 The pituitary gland

The pituitary gland is found in the pituitary fossa, also called Sella turcica because its similarity with a Turkish saddle (3). The pituitary fossa is a cavity located in the central region of the middle cranial fossa, positioned on the roof of the sphenoid sinus and is limited at the top by a fold of dura, also called diaphragm sella (3). The posterior boundary is formed by the dorsum sellae (3).

The gland consists of an anterior and a posterior lobe with an average adult weight of about 500–600 mg (4). The anterior and the posterior lobe differ both anatomically, as well as functionally and have different embryologic origins (5,6). While the anterior lobe origins from Rathke´s pouch the posterior lobe origins from the infundibulum of the diencephalon (4).

The anterior lobe can be subdivided into a pars distalis, a pars tuberalis and a pars intermedia (7). The pituitary gland relates to the hypothalamus through the infundibulum which is formed basal from the tuber cinereum and the recessus infundibularis (8). The anterior lobe of the pituitary gland covers the front of the pituitary infundibulum up to the tuber cinereum (8). Therefore, a proximal section can be identified, comprising the infundibulum and the infundibular portion of the anterior lobe, along with a distal section located within the sella turcica, which includes the anterior lobe, the posterior lobe, the pars intermedia and the pituitary cavity (8). The regulation of pituitary hormone secretion is influenced by hypothalamic neuropeptides delivered via the infundibular portal vessels, as well as by hormones from target organs (5). These signals either stimulate or inhibit systemic hormone release from the pituitary, which subsequently exerts endocrine and trophic effects on peripheral tissues (5). This area where hypothalamic neuropeptides are released, also called eminentia mediana, is lined by fenestrated endothelium and therefore facilitates the hypothalamic neuropeptides the transition into the blood (9).

The hypothalamus effects the hormone production of the anterior lobe of the pituitary gland through adenohypophysiotrophic hormones which are released into the hypothalamic portal system where they bind, G Protein cell surface membrane receptors, which are selective and specific for each hypothalamic hormone (5).

The posterior lobe is controlled by axon terminals which neurones are direct projections of the hypothalamus producing the hormones ADH and Oxytocin (7). The hormones are saved in granules and released into the bloodstream after a stimulus has taken place (9).

Hormonal production and function of the anterior lobe rely on the expression of specific transcription factors (10).

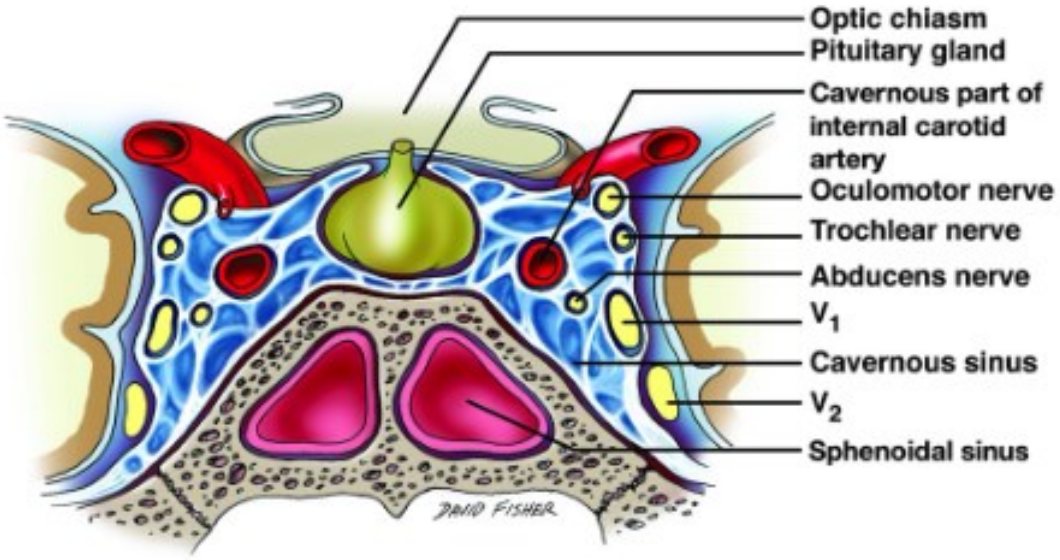

Figure 1: Relations of the pituitary gland by Balcerzak et al (2023) (11). © 2022 The Author(s). Published by Elsevier GmbH. This is an open access article under the CC BY-NC-ND license (http://creativecommons.org/licenses/by-nc-nd/4.0/).

The following cell lineages are relevant transcription factors for the anterior lobe and play a key role in the cytodifferentiation of stem cells in Rathke´s Pouch (10,12):

T-box transcription factor (TPIT):

- Differentiation into cortiocotroph cells (10,12).

Pituitary transcription factor 1 (PIT-1), Estrogen receptor α (Erα) and GATA-2 (13):

- Differentiation into somatotroph cells (10,12).
- Differentiation into lactotroph cells (10,12).
- Differentiation into thyrothroph cells (10,12).

Steroidogenic factor-1 (SF-1), Estrogen receptor α (ERα) and GATA-2 (13):

- Differentiation into gonadotroph cells (10,12).

These hormone-expressing pituitary cell lineages produce therefore different hormones (14) which differ also in their chemical structure (15). Hormones of the anterior lobe are the peptide hormones ACTH, GH and PRL which are constituted

of peptide chains (15). Further hormones of the anterior lobe are glycoprotein hormones LH, FSH and TSH with two subunits called alpha and beta (15).
The target of ACTH is the adrenal gland responsible for cortisol secretion (6). GH promotes growth and cell reproduction in many cells of the body, mainly due to the stimulating effect of IGF-1 secretion in the liver (15). Gonadal function and the secretion of androgens or estrogens is controlled by FSH and LH (6). TSH is involved in regulating metabolism through targeting the thyroid gland as well as the secretion of T4 (6). PRL stimulates the growth of the mammary gland leading to lactation of the female breast (15). Dysfunction and abnormalities of the pituitary function can result in hyper- or hyposecretion syndromes (6).

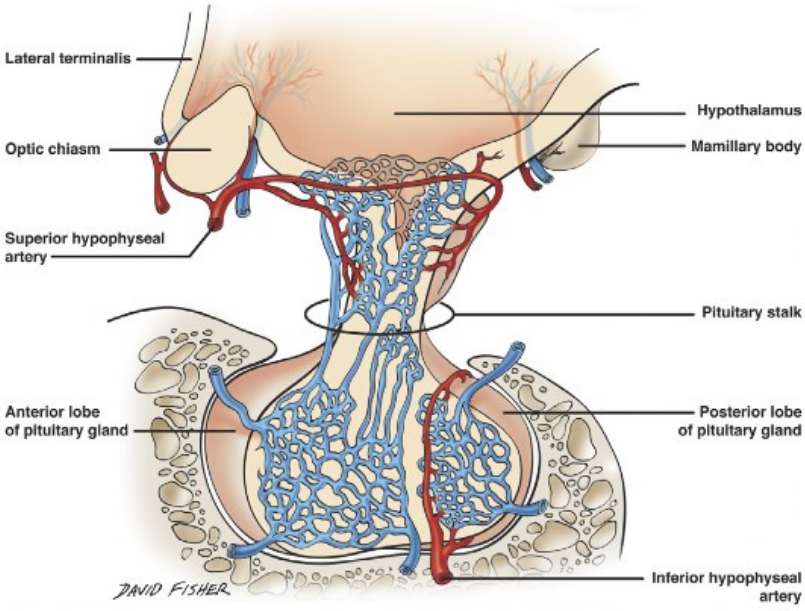

Figure 2: Arterial supply of the hypothalamus, pituitary stalk, pituitary gland and the sella turcica in a schematic drawing. Reprinted from Cironi et al (2020) (16) with permission from the Elsevier GmbH.

The pituitary gland receives its blood supply from multiple vessels (16). Originating from the ICA, the superior hypophyseal artery and the inferior hypophyseal artery supply the blood to the pituitary gland as well as providing the connection between the nervous and the endocrine-vascular system (8). Around the proximal part of the infundibulum, a ring like structure is formed by the left and right superior hypophyseal artery (8). The posterior lobe of the pituitary gland receives blood supply from the left and right inferior hypophyseal artery (8). The portal venous system drains blood from these vessels and leads the blood to the capillary network of the adenohypophysis, therefore the adenohypophysis receives no direct artery

blood supply (8) but hypothalamic neuropeptides reach the adenohypophysis without any delay (9). Venous blood from the pituitary gland is either drained indirectly via the intercavernous sinus or directly into the medial or inferior parts of the cavernous sinus (17). Further venous drainage occurs via the superior petrosal sinus, the inferior petrosal sinus and the sigmoid sinus into the internal jugular veins (11).

1.2 Pituitary adenoma

1.2.1 Classification

In most cases pituitary adenomas show a benign growth and arise from differentiated pituitary cell lineages (14). In a guideline from the European Society of Endocrinology, pituitary adenomas that show unusually rapid growth, are radiologically confirmed as invasive, and remain clinically relevant despite optimal standard therapy are classified as aggressive pituitary tumors (18). However, as soon as craniospinal and/or systemic metastasis are present, pituitary tumors are by definition carcinomas (18). These are extremely rare and account for only 0.2% of pituitary tumors (18).

In the past, histopathological findings, hormone content and ultrastructural features were used to classify adenomas (13). In the year 2017, Asa et al (2017) proposed to change the name from clonal adenohypophysial proliferations to pituitary neuroendocrine tumor PitNET (19), however this step was not without controversy (20).

The WHO Classification of 2017, was the first one to classify them into the three main cell lineages: PIT-1, SF-1 and T-PIT (13).

The main transcription factor for the acidophilic lineage is PIT-1 with other co-factors as ERα and GATA-2 leading into differentiation of somatotrophs (morphological variants: densely granulated adenoma, sparsely granulated adenoma, monocellular mammosomatotroph adenoma and bicellular mixed somatotroph-lactotroph adenoma), lactotrophs (morphological variants: sparsely granulated adenoma, densely granulated adenoma and acidophilic stem cell adenoma) and thyrotrophs adenohypophyseal cells (13).

The main transcription factor for the corticotroph lineage (morphological variants: densely granulated adenoma, sparsely granulated adenoma and crooke´s cell adenoma) is T-PIT leading into differentiation of corticotrophs adenohypophyseal cells (13).

For the gonadotroph lineage, relevant transcription factors are SF-1 with the co-factors Erα and GATA-2 leading into differentiation of gonadotrophs cells (13).

Pituitary adenomas lacking immunoreactivity for both pituitary hormones and transcription factors are now defined as null-cell adenomas (13). In contrast,

pituitary adenomas which show more than one hormonal expression in immunohistochemical examination are termed plurihormonal adenomas (13). Plurihomonal adenomas, however, cannot produce any hormones and represent as non-functioning (12).
In this thesis, pituitary adenomas are additionally classified according to the histo-pathological classification into the following subtypes: lactotroph, somatotroph, dual hormonal lactotroph and somatotroph, thyrotroph, corticotroph, gonadotroph, null-cell and plurihormonal adenomas (5,13).

1.2.1 Functional status

Pituitary adenomas can basically be divided into two groups: clinically functioning and non-functioning adenomas (12).
Prolactin secreting adenomas, also called prolactinomas show a prolactin level that exceeds the normal range of PRL in most cases above 150 ng per milliliter (14). In general, woman show a higher value of serum prolactin than men but assay-specific normal values are lower than 25 ng per milliliter (21). However, it must be mentioned that patients with other subtypes of pituitary adenoma, in most cases non-functioning adenomas, have elevated prolactin levels due to a compression of the infundibulum (22). Nonetheless, most patients with a non-functioning pituitary adenoma have prolactin levels below 100 ng per milliliter (23). Symptoms of prolactinomas range from amenorrhea, oligomenorrhea in women or oligospermia and azoospermia in men respectively galactorrhea in both sexes due to the constant suppression of gonadotropin (14).
Growth hormone secreting adenomas cause high levels of growth hormone, respectively IGF-1, responsible for the chronic multisystem disease of acromegaly (24). Typical symptoms of acromegaly are enlargement of the extremities of the peripheral body parts, cardiovascular disorders, osteoarticular disorders, metabolic manifestations, neuropathies or gastrointestinal manifestations (24). Acromegaly can be diagnosed by an oral glucose tolerance test (oGTT), administering 75 g glucose to the patient following measurement of the IGF-1 levels in the serum every 30 minutes for 2 hours after the administration to see if they are elevated and if there is no suppression of growth hormone (25).

Symptoms like moon facies with fragile skin, purple striae and increased bruising can be indicative of Cushing´s disease caused by a corticotropin-secreting corticotroph pituitary adenoma (14), named after the famous neurosurgeon Harvey W. Cushing. Recommended first-line tests for the diagnosis of Cushing's disease are serum cortisol tests including short and long-term tests as well as salivary and urine cortisol levels (26).

Thyrotropin-secreting pituitary adenomas are relatively seldom (approximately 2% of all pituitary adenomas), often diagnosed due to the size of the adenoma and not due a secondary hyperthyroidism (27).

If overproduction of hormones is not the cause of diagnosis and symptoms occur due to the mass of the adenoma, then pituitary adenomas are termed clinically non-functioning pituitary adenomas (28). In contrast, silent adenomas are producing hormones but a clinically relevant level is not reached (28). A majority of the adenomas in this group originate from the gonadotroph lineage (14).

These adenomas are often macroadenomas and cause symptoms due to their size and compression of the surrounding anatomical structures (14,28,29).

Clinically these adenomas often present with: headache in the frontal and occipital region due to the stretching of the diaphragm; bitemporal visual defects due to the compression of the opto-chiasmatic system; hormone deficiencies; hyperprolactinemia or diabetes insipidus due to the compression of the normal pituitary gland, the infundibulum and portal vessels (22).

1.2.3 Size and invasion

Pituitary adenomas can further be categorized based on their size seen on MRI-scans (12). If the diameter is less than < 10 mm, the adenoma is classified as micro- and if the diameter is above > 10 mm, the adenoma is classified as macroadenoma (12). Furthermore, adenomas larger than 40 mm are termed giant adenomas (12).

Pituitary adenomas are capable of infiltrating adjacent structures such as bone, dura mater or the sphenoid sinus (1,2). The degree of invasion into the parasellar space, particularly into the CS, is a significant prognostic element for both surgical outcome and recurrence (1,2). Other important factors are growth rate, size respectively volume or the histopathological subtype (2). However, a distinction should be made

between true invasion, e.g. infiltrative growth into the CS or solely a displacement of parasellar structures because of the tumor mass (2).

1.3 The cavernous sinus

Found in the middle cranial fossa, the CS is defined as a paired dural venous sinus which contains the pituitary gland (11). The size in a human adult is about 1 cm in width and 2 cm in length (11).

In an examination of specimen, Bergland et. al (1968) described that 85% of the examined cases had an anterior intercavernous sinus while behind or beneath the pituitary gland an intercavernous sinus was seen less often (30). The CS is positioned between the endosteal and meningeal layers of the dura mater (11). Overview of anatomical boundaries of the CS according to Rhoton et. al (2002) (31):

- Anterior: medial end of the superior orbital fissure of the sphenoid bone (31) covered with a continuation of the periosteal layer of dura mater forming the anterior wall of the CS (32).
- Posterior: pars petrosa of the temporal bone covered with two layers of dura mater (11).
- Superior: meningeal layer of dura mater which is connected to the anterior and middle clinoid process (31) forming the dural diaphragm (33).
- Medial: meningeal layer of dura mater forming the medial wall of the CS, connected with a thin layer of connective tissue to the pituitary gland (33).
- Lateral: the floor of the sphenoid bone (of the middle cranial fossa) to the roof of the basal cisterns also facing the temporal lobe (11,31).
- Inferior: the sphenoid bone covered with periosteal layer of the dura mater (11).

The CS is also in close relation to important structures and vessels of the central nervous system (11).

- Superior: the opto-chiasmatic system and the ICA (11).
- Medial: the pituitary gland (11).
- Inferior: sphenoidal sinus (11).
- Lateral: the temporal lobe with the uncus (11).
- Anterior: the superior orbital fissure and orbit (11).

The CS has several connections to surrounding veins (11), which includes the basal cerebral veins, the spheno-parietal sinus and the superficial middle cerebral vein (34). The venous inflow from the superior ophthalmic vein is of clinical importance due to anastomoses with the facial and angular veins (34).
The CS also includes clinically relevant structures such as the cavernous part of the ICA, the abducens nerve as well as the oculomotor nerve, the trochlear nerve, the ophthalmic nerve and the maxillary nerve which course between the superficial and deep layers of the lateral wall of the CS (11).

Origination from the common carotid artery, running through the canalis caroticus of the petrous temporal bone, the ICA runs through the cavernous sinus while entering the skull (34). The ICA makes two turns within the CS. The first one can vary in its geometry while the second turn, called the carotid siphon, is a bend of 45 degrees resulting in a reversal of the artery´s direction of flow (35). Fernandez-Miranda et. al (2018) summarized the course of the parasellar ICA as follows: entering the CS short vertical, posterior genu, horizontal and anterior genu (32). The comprehensive review of Balzercak et. al (2023) evaluated 8 classifications systems of the ICA and finally chose the classification system of Bouthiller et al. (1996), being most often mentioned in publications and due to its common acceptance in clinical use (11,36).

1.4 Compartments of the cavernous sinus

The following chapters deal with the four cavernous sinus compartments which are defined due to their relationship with the cavernous ICA based on the work of Fernandez-Miranda et. al (2017) and Xu et. al (2024). In the process of their work, Fernandez-Miranda et. al (2017) used 25 colored silicon-injected human head specimens to develop an anatomy-based classification which complements current imaging-based classifications (32) while Xu et. al (2024) illustrated the anatomical landmarks of the lateral compartment of the CS (37).

1.4.1 Superior compartment of the CS

As figure 3 shows, the superior compartment is found between the horizontal section and the anterior genu of the cavernous ICA (32). The upper anatomical limit of the superior compartment is the roof of the CS (32), which is defined as a meningeal layer of dura mater connected to the anterior and middle clinoid process (11). The oculomotor triangle forms the posterolateral anatomical limitation (32) and is formed by the anterior petroclinoidal ligament, the posterior petroclinoidal ligament and the interclinoidal dural ligament (38).

The anterior petroclinoidal ligament connects the petrous apex with the anterior clinoid process while the posterior petroclinoidal ligament connects the petrous apex with the posterior clinoid process (39). Extending from the posterior to the anterior clinoid process, the interclinoidal ligament, defined as a dural band, is a very important structure at the roof of the superior compartment (32). The separation of the oculomotor triangle and the clinoidal triangle is also performed by the interclinoidal ligament (32). First defined by Dolenc (40), the clinoidal triangle is formed by the CN II, the CN III and the anterior clinoid process in the area where the tentorium is anchored (41). Another important structure of the superior compartment is the CN III, running laterally to the interclinoidal ligament between two layers of dura before entering the CS laterally to the anterior genu of the ICA (32). The distal dura ring is shaped laterally by the dural continuation from the superior surface of the anterior clinoid process, anteriorly by the dural continuation below the optic nerve and above the optic strut while medially the dural continuation located above the optic strut reaches in the direction of the ICA (39).

Illustration of the anatomical relationships with explanation of the individual points of figure 3:

A: In a view from medial to lateral the oculomotor nerve runs lateral to the interclinoidal ligament as well as in the lateral wall of the superior CS compartment (32). Forming the posterolateral border of the superior CS compartment, the oculomotor triangle can also be seen (32).

B: Running between the superficial and deep layers of the lateral CS wall - the interdural segment of the oculomotor nerve.

C, D: The interclinoidal ligament and the oculomotor nerve without and with mediolateral displacement of the ICA (32). As mentioned above, the posterolateral border of the superior CS compartment formed by the oculomotor triangle (32). Also visible here, the horizontal section of the ICA, the anterior genu, the paraclinoidal section of the ICA and the extra- and intradural section of the oculomotor nerve (32).

E, F: MRI-scan showing the pituitary adenoma invasion into the superior and inferior compartment of the CS (32). Coronal plane in E and saggital plane in F (32). This total encasement of the cavernous ICA corresponds to Knosp Grade 4 (42).

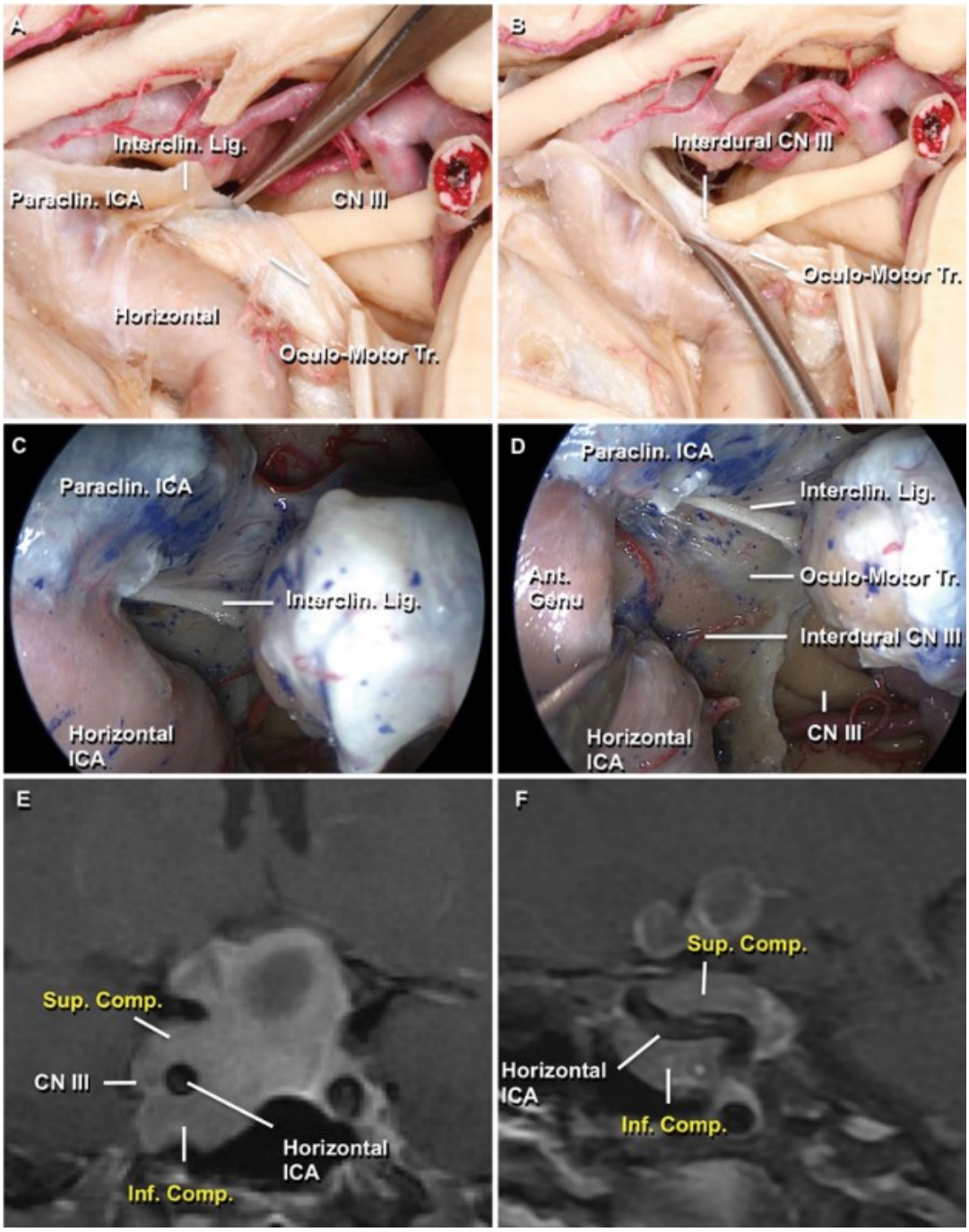

Figure 3: Anatomical relationship of the superior CS compartment. Reprinted from Fernandes-Miranda et al. (2018) (32) with permission from the American Association of Neurological Surgeons.

1.4.2 Posterior compartment of the CS

The boundary of the posterior compartment is formed by the petroclival dura while the compartment itself is located behind the short vertical cavernous ICA, the horizontal part of the cavernous ICA indicates the transition to the superior compartment already (32). To understand the anatomical conditions of the posterior

compartment the course of the abducens nerve is of importance. Laconetta et. al (2003) named the section after the intradural part (running between the dura mater and the periosteum of the clivus) of the abducens nerve which courses into a venous space, filled with blood from the cavernous sinus, the basilar plexus and the superior petrosal sinus the sphenopetroclival venous gulf (43,44).

The further course of the gulfar section up to the CS is passing the Dorello´s canal to course between the petro-sphenoidal ligament and to enter the CS laterally to the posterior genu of the ICA (44). The Dorello Canal, named by Dorello et al (1905), is formed by the petro-sphenoidal ligament, the petrous apex, the lateral aspect of the inferior dorsum sellae and the superior aspect of the clivus and contains the abducens nerve (44). This gulfar section of the abducens nerve is found at the bottom of the posterior compartment and sits above the sphenopetroclival venous gulf (32).

The cavernous section of the abducens nerve extends from the entrance to the CS, running laterally and fixed to the horizontal section of the cavernous ICA as well as the beginning of the anterior genu, up to the superior orbital fissure (44). Another structure, arising from the ICA at the height of the posterior genu in the posterior compartment, is the meningohypophyseal trunk (32).

Illustration of the anatomical relationships with explanation of the individual points of figure 4:

A: Visualization and localization of the posterior CS compartment with its key structures: short vertical section of the ICA, posterior genu of the ICA, the proximal cavernous section of the abducens nerve and the meningohypophyseal trunk arising from the ICA at the level of the posterior genu (32).

B: Below the dissector, the gulfar section of the abducens nerve can be seen located at the bottom of the posterior compartment (32).

C: Another visualization of the gulfar section of the abducens nerve above the petrous apex as well as the sphenopetroclival venous gulf (32). Displacement of the short vertical ICA makes the visualization of the cavernous section of the abducens nerve possible (32).

D: Saggital plane MRI-scan showing the pituitary adenoma invasion into the posterior and inferior compartment of the CS (32).

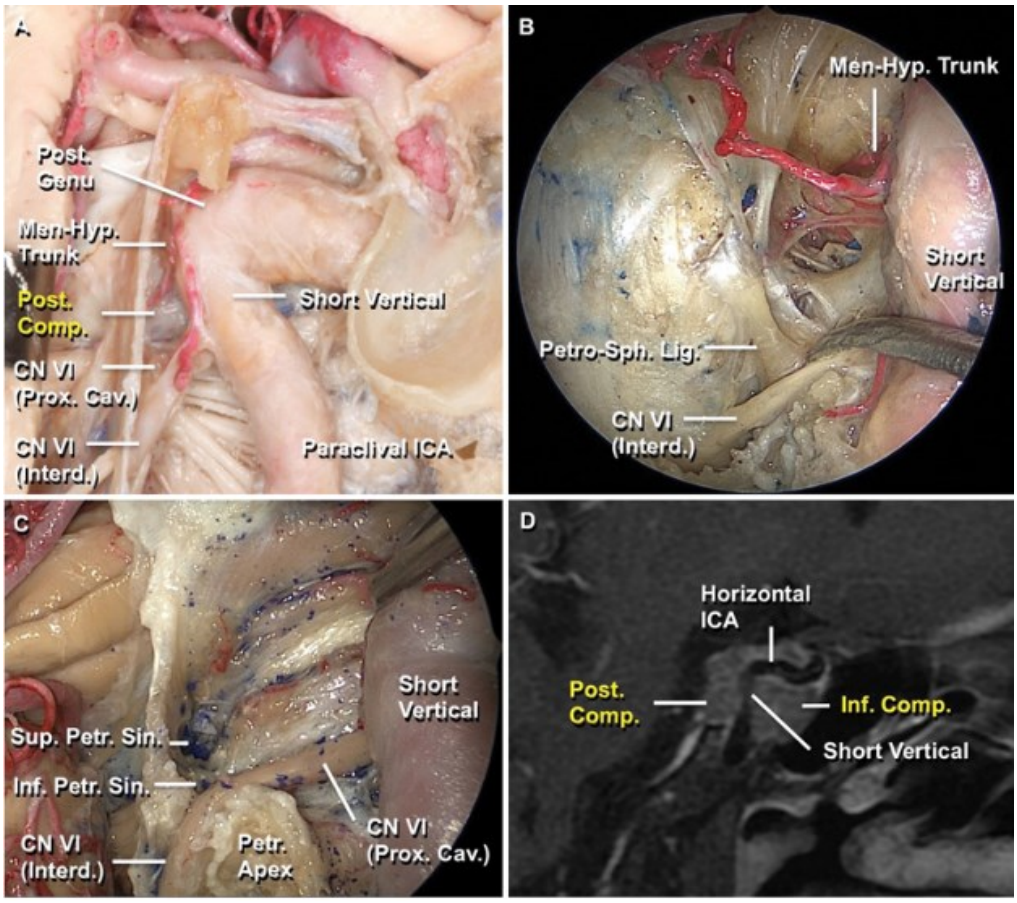

Figure 4: Anatomical relationship of the posterior CS compartment. Reprinted from Fernandes-Miranda et al. (2018) (32) with permission from the American Association of Neurological Surgeons.

1.4.3 Inferior compartment of the CS

Boundaries of the inferior compartment of the CS are: superior the horizontal and anterior genu sections of the ICA as well as posterior the short vertical section of the ICA (32). As mentioned above, the anterior wall of the CS is a continuation of the periosteal layer which also envelops the pituitary gland (32). The lateral border of the inferior compartment is marked by the abducens nerve, running lateral to the horizontal ICA (32). Furthermore, the sympathetic nerve located medially to the abducens nerve is running diagonally from the short vertical segment of the ICA to the horizontal section of the ICA through the inferior compartment (32).

Illustration of the anatomical relationships with explanation of the individual points of figure 5:

A: Meningeal layer of dura mater forming the medial wall of the CS, attached with a thin layer of connective tissue to the pituitary gland (32). Periosteal layer of dura mater forming the anterior wall of the CS (32).

B: The CS is represented by the blue silicone (32).

C: Visualization of the inferior compartment in a medial view and its relationship with the horizontal section of the ICA, vertical section of the ICA, the distal cavernous abducens nerve and the sympathetic nerve (32).

D: Seen from a slightly different angel, the floor of the CS and again the distal cavernous abducens nerve as well as the sympathetic nerve (32).

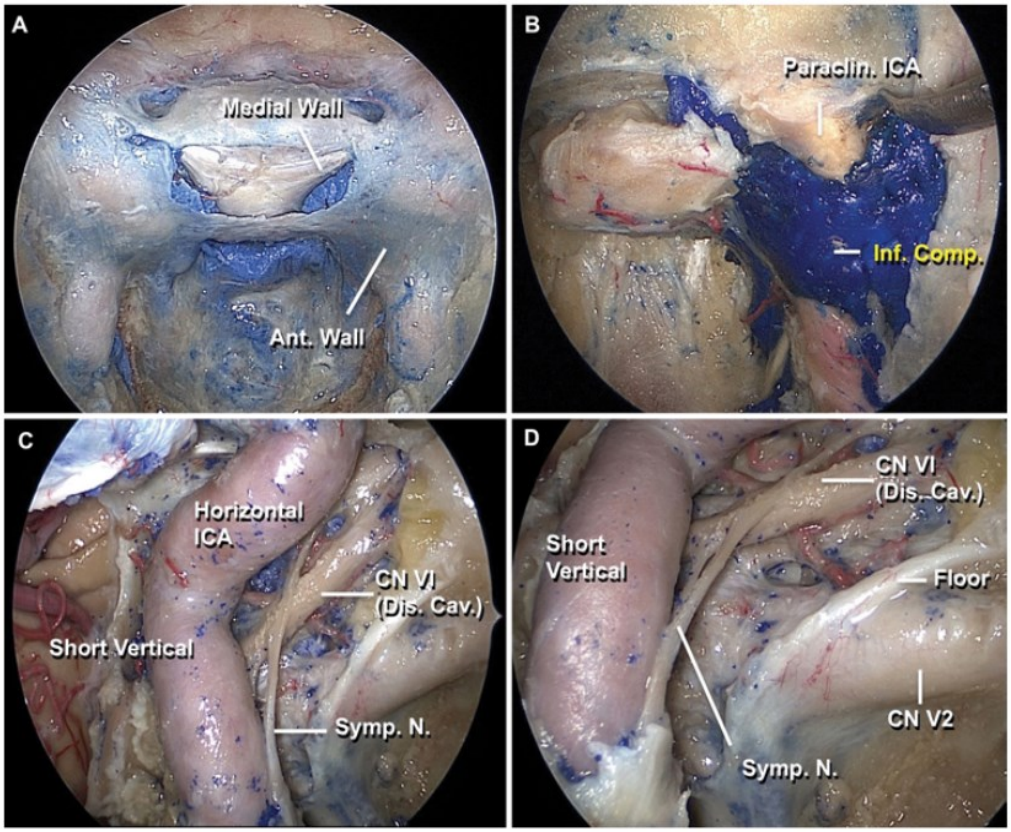

Figure 5: Anatomical relationship of the inferior CS compartment. Reprinted from Fernandes-Miranda et al. (2018) (32) with permission from the American Association of Neurological Surgeons.

1.4.4 Lateral compartment of the CS

The lateral compartment of the CS is located between the ICA and the lateral wall of the CS and is bounded at the top by the carotid-oculomotor membrane, the proximal dura ring and the posterior clinoid process (37). The inferior anatomical boundaries are the maxillary nerve, the maxillary strut defined as a bone separating the foramen rotundum and the superior orbital fissure (45), the petrolingual ligament and the lingual process of the sphenoid bone while posterior the petrous apex represents the anatomical landmark (37). Between the lateral wall of the CS and the ICA, Xu et al. (2024) could find well-defined ligamentous bands in their work and defined them as lateral parasellar ligaments (37). Two characteristics of these bands were observed: robust and adherent to the ICA or dispersed bands with less adherence, mostly attached to the horizontal section of the ICA (37). Furthermore, the inferior lateral trunk, a vessel originating from the horizontal section of the ICA and supplying the ocoulomotor, trochlear and abducens nerve (46), was identified in 93.2% of their cases (37). Together, the lateral parasellar ligaments, the sympathetic nerve and the inferior lateral trunk form the neurovascular-ligamental complex (37).

Furthermore, Xu et al. (2024) proposed to divide the lateral compartment of the CS into two subcompartments. The border between these two compartments represents the abducens nerve (37). In the upper subcompartment the inferior lateral trunk and the parasellar ligaments can be found while the sympathetic nerve is in the lower subcompartment (37). Point A of Figure 6 illustrates the right lateral compartment of the CS in an endoscopic approach while point B of figure 6 shows the left lateral compartment from a microsurgical approach (37).

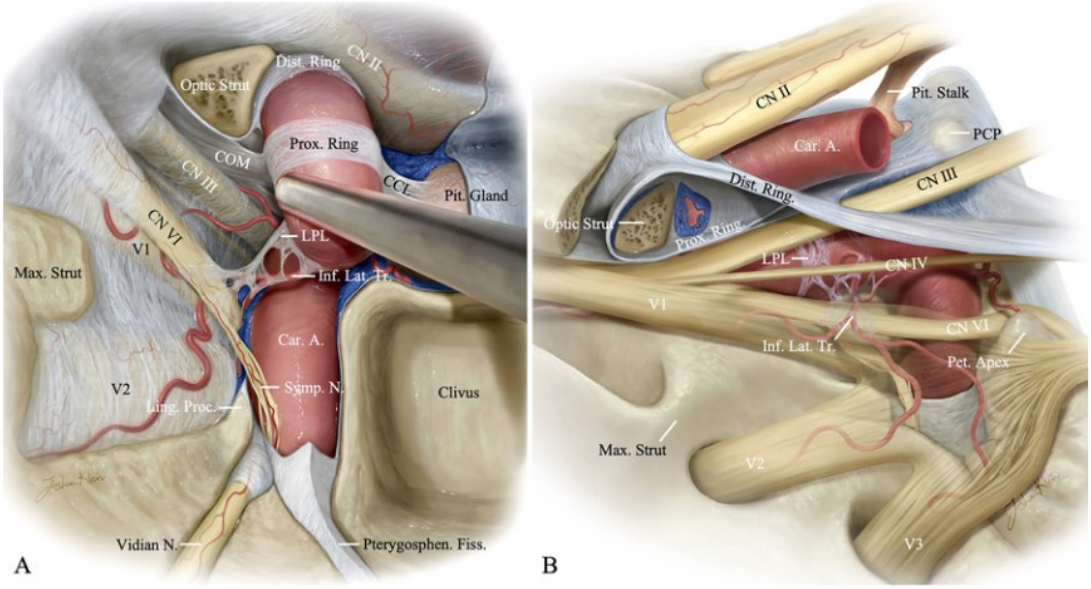

Figure 6: Anatomical relationship of the lateral CS compartment reprinted from Xu et al. (2024) (37). © Juan Carlos Fernandez-Miranda, MD, and Aaron Cohen-Gadol, MD, published with permission.

1.5 The posterior clinoid process

Forming the posterior boundary of the sella turcica, the dorsum sellae is above the upper clivus which is part of the sphenoid bone (47). The bony protuberance located at the superior and lateral aspect of the dorsum sellae is defined as the posterior clinoid process (48) and is an important structure in the parasellar region (49). The posterior clinoid process has anatomical relationships with the CN III which runs laterally from the clinoid process (49). The posterior communicating artery runs superiorly as well as with the clinoid section of the ICA in front of the clinoid process (49). The clinoid process is covered by the continuation of the periosteal dura of the sella floor, while the continuation of the meningeal layer of the medial wall covers the clinoid process too (49). Serioli et al. (2023) found, that in 44% of cases an interclinoid ligament was present, which connects the anterior and posterior clinoid process (50). In the remaining cases, however, it was indistinguishable from the roof of the CS (50). It is also possible that the interclinoid ligament is ossified and therefore a bony fusion between the anterior clinoid process and the posterior clinoid process is present (51). Asem et al. (2011) radiologically evaluated 36 adult cadaveric heads and could find various variations of the posterior clinoid process such as: a complete absence or a fusion between the anterior and posterior process

(51). Another ligament which is related to the posterior clinoid process is the caroticoclinoid ligament arising like a fibrous bundle from the medial wall of the cavernous sinus attaching to the anterior genu of the ICA, the middle clinoid process and the posterior clinoid process (49). The proximal dura ring is therefore a continuation of the caroticoclinoid ligament after the anterior clinoid process (49) while the carotid-oculomotor membrane can be seen as a continuation of the caroticoclinoid ligament after the anterior genu of the ICA (50).

1.6 The medial wall of the CS

As described by Sertoli et al. (2023), the medial wall of the CS is subject to scientific discussion (50). The question is whether the medial wall is a single meningeal layer of dura mater, a loose fibrous tissue or an own thin pituitary gland collagen capsule layer (52,53). The systematic review by Gonçalves et al. (2012) summarized, that a consensus on this matter can only be reached once further studies are published (52). However, Yasude et al. (2004) could determine that there is a single layer of dura mater separating the CS from the capsule of the pituitary gland (54). Troung et al. (2019) could identify well-defined dura-like membranes, which are attached with a thin layer of arachnoid-like bands of connective tissue to the pituitary gland, in all their cases (33). These well-defined dura-like membranes are attached by ligamentous dura-like trabeculae to the anterior and lateral walls of the cavernous sinus, the ICA and the anterior clinoid process (33). Troung et al. (2019) classified these parasellar ligaments into the previously described caroticoclinoid ligament as well as into the superior, inferior and posterior parasellar ligaments (33).

1.7 Knosp Grading

To find radiological criteria that indicate invasion of the CS, Knosp et. al (1993) developed a new grading system for pituitary adenomas with surgically microscopic view proven invasion (42). With a “midsella” coronal MRI-scan, the cross-sections of the intracavernous and the supracavernous ICA can be displayed well (42).
This MRI-scan based classification was evaluated by Micko et al. (2015) with direct endoscopic visualization of the medial wall of the CS (2). With this technique, the invasiveness of pituitary adenomas into the CS could be observed better and invasion into the inferior compartment was observed more often than invasion into the superior compartment of the CS (2).
Therefore, the authors decided to split grade 3 into 3A (superior compartment) and grade 3B (inferior compartment) (2).
This grading system was used to classify all pituitary adenomas in our study.

Grade 0:
This grade stands for the normal condition of the CS space. As figure 7 A shows, the medial aspects of the supra- and intracavernous ICA are not passed by the adenoma (42).
Grade 1:
Drawing a line between the cross-sectional-centers of the ICA was termed the intercarotid line. Figure 7 B of Grade 1 shows that this line between the cross-sectional-centers of the supra- and intracavernous ICA is not passed by the adenoma (42).
Grade 2:
In grade 2, the tumor projects beyond the intracarotid line, however the adenoma does not go beyond the lateral tangent of the supra- and intracavernous ICA. This status is illustrated by figure 7 C (42).
Grade 3A:
This grade shows the growth of the adenoma into the superior compartment of the CS. Therefore, the adenoma does go beyond the lateral tangent of the supra- and intracavernous ICA. Figure 7 D (42).

Grade 3B:

As figure 7 E shows, the adenoma is extending into the inferior compartment of the CS and does go beyond the lateral tangent of the supra- and intracavernous ICA (2).

Grade 4:

In grade 4 a total encasement of the intracavernous artery has to be present (42).

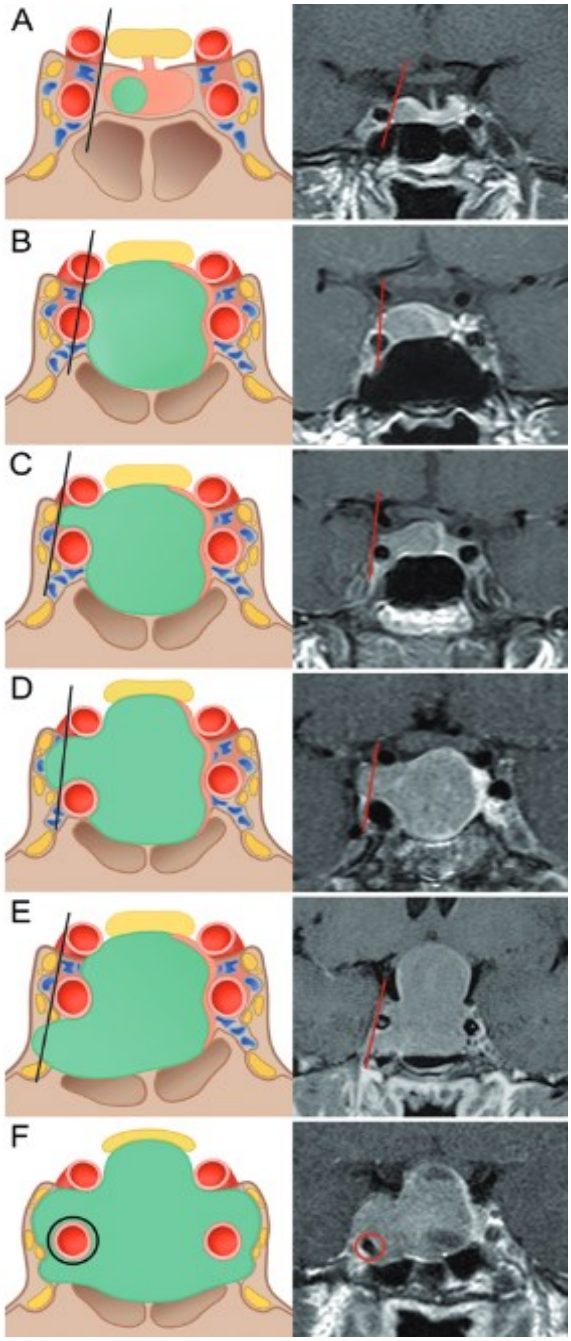

Figure 7: Revised Knosp Grading by Micko et al. (2015) (29) © Prof. Dr. Knosp Engelbert, published with permission.

2. Methods and materials

2.1 Method

The aim of the diploma thesis was to demonstrate a statistical correlation between invasion of pituitary adenomas into the compartments of the CS and morphological characteristics. This retrospective analysis of patient data includes 273 patients who underwent endoscopic transnasal transsphenoidal surgery for pituitary adenoma between 2013 and 2022 at the Department of Neurosurgery, Medical University of Graz.

The ethics committee of the Medical University of Graz approved this study (EK number: 36-004 ex 23/24).

The following hypotheses were proposed:

H_0-hypothesis: There is no statistical correlation between the invasion of pituitary adenomas into the CS and the morphology of the adenoma.

H_1-hypothesis: There is a statistical correlation between the invasion of pituitary adenomas into the CS and the morphology of the adenoma.

2.2 Data collection

The data was collected from the KAGes (Styrian state hospitals and state care centers) hospital information system (openMEDOCS). All personal data were pseudonymized to comply with data protection. Therefore, the patient-s´ electronic medical records and operation reports from the Department of Pathology, the Department of Internal Medicine - Division of Endocrinology-Diabetology and the Department of Neurosurgery of the Medical University of Graz, were evaluated.

The sellar and parasellar structures were analyzed using the Medtronic S8 Navigation system (Medtronic, Colorado, USA). Therefore, we created a multimodality model with 1,5- or 3.0-Tesla scanner images of: enhanced T1-weighted MPRAGE-MRI-protocols for soft tissue structures and MRA-time of flight protocols for the visualization of the vessels (55). In addition, since 2022 VIBE- and CISS-MRI-protocols were applied (55), respectively computed tomography images for bone structures and the sphenoid anatomy (56).

Inclusion criteria consisted of age between 18–80 years and histopathological confirmed pituitary adenoma tissue. Patients outside of this age range,

histopathological diagnoses other than pituitary adenoma tissue (such as meningiomas or craniopharyngiomas) as well as re-operation of a patient who had already primarily been operated before 2013, were excluded.

The following data were collected:

- Age
- Number of operations
- Post-operative radiotherapy (for residual or recurrent adenomas)
- Size of the adenoma in mm (12)
- Volume of the adenoma in cm^3
- Displacement of the left and right ICA in mm (57)
- Presence of the posterior clinoid process (51)
- Revised Knosp Grading (2)
- Hardy Grading (58,59)
- Histopathological subtype of pituitary adenoma (EMR) according to the 2017 WHO Classification of Endocrine Organs done at the department of pathology (60)
- MIB-1 Antibody (EMR) done at the department of pathology (61)
- Functional status (12)
- Endoscopically observed invasion into the CS (2), judged intraoperatively by the operating neurosurgeon
- Pituitary adenoma consistency (62,63), judged intraoperatively by the operating surgeon
- Degree of resection judged intraoperatively by the operating surgeon (64)
- Remission (1,65)
- Duration of follow-up in months

2.2.1 Preoperative data collection

The patient characteristics (such as age at time of surgery) of all pituitary operations were retrieved from the electronic medical records system. To determine whether the adenoma was hormonally active and therefore hormonal hypersecretion or signs and symptoms of hypersecretion were present (12), we reviewed the preoperative

findings of the Department of Internal Medicine - Division for Endocrinology and Diabetology of the Medical University of Graz.

Imaging data of preoperative magnetic resonance images as well as computed tomography images were analyzed with the Medtronic S8 Navigation system (Medtronic, Colorado, USA). This allowed us to evaluate axial, coronal and sagittal planes after multiplanar reconstruction of the MRI- and CT-scans. The grading of the parasellar extension was done, as described above, by the revised Knosp Grading (2) and the suprasellar extension by Hardy Grading (58,59).

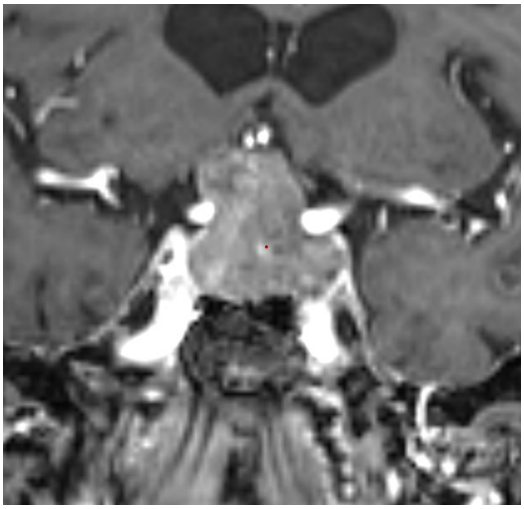

Figure 8: Assessing the Knosp Grade with a midsella Coronal T1-weighted contrast-enhanced MRI-scan using the Medtronic S8 Navigation system (Medtronic, Colorado, USA).

The volume of the pituitary adenoma was computed with the Medtronic S8 Navigation system (Medtronic, Colorado, USA) using the automatic 3D model measurement respectively manually refining the adenoma in each coronary section to generate a 3D model.

To categories the size of the pituitary adenoma, we measured the longest diameter of the adenoma. If the diameter was less than < 10 mm, the adenoma was classified as micro- and with a diameter above 10 mm was classified as macro adenoma (12).

To evaluate whether the posterior clinoid process was visible, we reviewed the CT-scans in the sagittal and coronal planes. If there was no bone structure arising from the middle of the sellar floor, the posterior clinoid process was declared as absent (51).

In order to measure the displacement of the cavernous ICA by the adenoma (57), we created a reference line through the falx cerebri with the Medtronic S8 Navigation system (Medtronic, Colorado, USA) in a midsella coronal section MRI-scan. After that, we drew a horizontal line from the center of the right and left cavernous ICA to our reference line and measured the distance in millimeter. For the side with the longer distance to the cavernous ICA, displacement was declared.

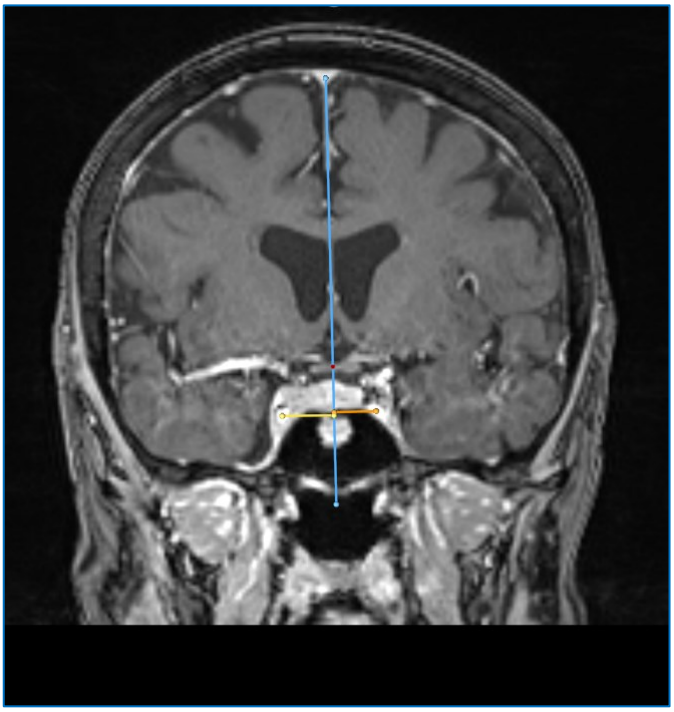

Figure 9: Coronal T1-weighted contrast-enhanced MRI-scan. Measuring the displacement of the cavernous ICA with a midsella coronal section T1- MRI-scan using the Medtronic S8 Navigation system (Medtronic, Colorado, USA). Yellow - distance left 14.4 mm, Orange - distance right 11.6 mm.

2.2.2 Postoperative data collection

All histopathological confirmed pituitary adenoma tissues were examined post-operatively by the Department of Pathology of the Medical University of Graz, according to the classification of the WHO from 2017 (Tumors of Endocrine Organs) (60). This has been done using hematoxylin and eosin as well as immunohistochemistical staining of the main pituitary hormones and pituitary transcription factors (13). Furthermore, the proliferation rate was evaluated using the MIB-1 antibody/Ki-67 index (61).

Thus, the pituitary adenomas were divided into the following histopathological subtypes:

- Somatotroph (GH)
- Lactotroph (PRL)
- Somatotroph and lactotroph (GH + PRL)
- Thyrothroph (TSH)
- Corticotroph (ACTH)
- Gonadothroph (LH / FSH)
- Null cell (0-cell)
- Plurihormonal (PLURI)
- Apoplectic

From the neurosurgeon´s operation report, we were able to collect the following data: consistency of the adenoma categorized into the groups cystic, soft, average, firm and calcified (63). For the statistical analysis, we summarized the groups cystic, soft and average as “soft - suckable” adenoma tissue (62). Therefore, the groups of firm and calcified pituitary adenomas where summarized as “fibrous - unsuckable” adenoma tissue (62).

If the neurosurgeon detected adenoma tissue within the CS space, a medial wall that was no longer intact or visible, structures of the CS, or the adventitia of the cavernous ICA, the adenoma was declared as invasive (2).

If an adenoma was described as invasive, we also analyzed the neurosurgeon´s operation report to evaluate if the consistency of the tissue within the CS was different in comparison to the main tumor consistency (1).

The degree of resection was categorized into: total (100%), subtotal (99–80%) and partial (< 80%) (64).

Surgical cure and respectively of functional adenomas was defined based on the work of Micko et al. (2017) (65). Remission of nonfunctional adenomas was declared if no residual or recurrent pituitary adenoma was visible at the last MRI-follow-up (1).

Post-operative radiotherapy data (for residual or recurrent adenomas) was collected from the electronic medical records.

2.3 Statistical analysis

For statistical analysis we used SPSS version 29.0, (SPSS Inc., IBM, Armonk, New York, USA). Two study groups were defined based on the decision if the tumor showed signs of invasiveness into the CS (Group: Invasion) or not (Group: Non-Invasive). In order to compare these two groups, we used either the chi-square test or the Fisher´s exact test for binary variables. Metric variables were compared by using the unpaired t-test and in case of a non-normal distributed variable the Mann-Whitney-U test. The binominal multivariate regression test was used to analyze the influence of several independent variables on our binary dependent variable “invasion into the CS”.

The chi-square test or the Fisher´s exact test was used for the following variables: functional status of pituitary adenoma (non-functioning / functioning), Knosp Grade, Hardy Grade, histopathological subtypes, consistency of the adenoma, degree of resection and remission.
The unpaired t-test or the Mann-Whitney-U-test was used for: age, volume, size and follow-up (in months).

A binomial multivariate logistic regression model determined the effect on endoscopically observed invasion as well as control for potential confounding factors. For this model, we only tested pituitary adenomas that were larger than 10 mm in diameter (macroadenoma). Therefore, we tested the effect of consistency of the adenoma (soft / fibrous), age (< 60, > 60), volume of the adenoma which was separated into five dichotomous groups, displacement of the left and right ICA (no / yes), presence of the posterior clinoid process (no / yes) and functional status (non-functioning / functioning) on “invasion into the CS”.
To determine a statistically significant association between volume and “invasion into the CS”, each dichotomous volume group was tested with the other factors in a separate binomial multivariate logistic regression model.

The five dichotomous groups tested in this model were as follows:

- < 0.6 cm^3, > 0.6 cm^3
- < 0.7 cm^3, > 0.7 cm^3
- < 0.8 cm^3, > 0.8 cm^3
- < 0.9 cm^3, > 0.9 cm^3
- < 1 cm^3, > 1 cm^3

In addition to the binomial multivariate logistic regression model for macroadenomas, a multivariate binomial logistic regression model was used to establish a correlation between volume and invasiveness in non-functioning adenomas. Therefore, we tested the effect of consistency of the adenoma (soft / fibrous), age (< 60, > 60), volume of the adenoma which was separated into six dichotomous groups, displacement of the left and right ICA (no / yes) and presence of the posterior clinoid process (no / yes) of the pituitary adenoma on “invasion into the CS”. To determine a statistically significant association between volume and “invasion into the CS”, each dichotomous volume group was tested with the other factors in a separate binomial multivariate logistic regression model.
The six dichotomous groups tested in this model were as follows:

- < 1 cm^3, > 1cm^3
- < 1.2 cm^3, > 1.2 cm^3
- < 1.3 cm^3, > 1.3 cm^3
- < 1.4 cm^3, > 1.4 cm^3
- < 1.5 cm^3, > 1.5 cm^3
- < 1.6 cm^3, > 1.6 cm^3

A moderation analysis was performed using the PROCESS macro by Hayes (2018) (66) to determine the effect of the volume in cm^3 and the interaction with invasion of the pituitary adenoma to predict the displacement of the left and right cavernous ICA in mm. Therefore, we created a moderated regression model with the moderation term “invasion into the CS”.

A significance level of p = < 0.05 was assumed for all tests.

3. Results

3.1 Baseline characteristics

From 2013 to 2022, 273 patients were operated by a pure endoscopic approach at the Department of Neurosurgery, Medical University of Graz due to a pituitary adenoma. In 8 cases, no operation report was available and therefore 265 patients were included for further analysis in this study.

In group “non-invasive” (Group: Non-Inv), no endoscopically observed invasion into the CS was detected in 165 cases (62.3%), whereas clear signs of invasion (Group: Inv) were found in 100 cases (37.7%). In group Non-Inv 53.9% of the patients were women and 41.1% were men while in group Inv 43% of the patients were women and 57% were men (p = 0.084). For the remaining cases, no information on invasion into the CS was available.

The average age of patients in the group Non-Inv was mean 54.8 years (Standard deviation, SD: ± 14.84) and in the group Inv 58.2 (SD: ± 13.2, p = 0.055).

In group Non-Inv 10 pituitary adenomas (6.1%) were microadenomas, whereas no microadenoma was found in group Inv (0%, p = 0.008). The median size of pituitary adenomas in group Non-Inv was 20.3 mm (IQR: 14.9–27.5), in group Inv 29 mm (IQR: 20–38.4, p = < 0.001). The median volume was 2.5 cm^3 (IQR: 1.2–6.7) in group Non-Inv and 7.3 cm^3 (IQR: 2.8–13.3) in group Inv (p = < 0.001).

Overall, 120 cases (72.7%) in group Non-Inv were non-functioning pituitary adenomas and 45 (27.3%) were functioning pituitary adenomas. In group Inv 75 (75%) were non-functioning and 25 (25%) were functioning pituitary adenomas (p = 0.684). (**Table 1**)

Table 1: Baseline characteristics of the two study groups, comparing no endoscopically observed invasion (Group: Non-Inv) and invasion into the CS (Group: Inv).

	NON-INV	INV	P-VALUE
NUMBER	165	100	
SEX			0.084
MALE	76 (46.1%)	57 (57%)	
FEMALE	89 (53.9%)	43 (43%)	
AGE (MEAN)	54.8 (SD ± 14.84)	58.2 (SD ± 13.2)	0.055
FUNCTIONAL STATUS			0.684
NON-FUNCTION.	120 (72.7%)	75 (75%)	
FUNCTIONING	45 (27.3%)	25 (25%)	
VOLUME (MEDIAN)	2.5 (IQR: 1.2–6.7)	7.3 (IQR: 2.8–13.3)	**< 0.001**
SIZE			**0.008**
MICROADENOMA	10 (6.1%)	0	
MACROADENOMA	155 (93.9%)	100 (100%)	
SIZE (MM) (MEDIAN)	20.3 (IQR: 14.9–27.5)	29.0 (IQR: 20–38.4)	**< 0.001**
DISPLACEMENT OF THE RIGHT ICA IN MM (MEAN)	12.364 (SD ± 2.706)	13.040 (SD ± 3.081)	0.064
DISPLACEMENT OF THE LEFT ICA IN MM (MEAN)	13.493 (SD ± 2.596)	14.209 (SD ± 2.853)	**0.038**
KNOSP GRADING			**< 0.001**
0	62 (37.6%)	23 (23%)	
1	38 (23%)	17 (17%)	
2	32 (19.4%)	14 (14%)	
3A	25 (15.2%)	22 (22%)	
3B	4 (2.4%)	5 (5%)	
4	4 (2.4%)	19 (19%)	
HARDY GRADING			0.322
0	48 (29.1%)	26 (26%)	
A	70 (42.4%)	35 (35%)	
B	42 (25.5%)	35 (35%)	
C	5 (3%)	3 (3%)	
D	0	1 (1%)	
HISTO. SUBTYPES			0.925
ACTH	24 (14.5%)	15 (15%)	
GH	14 (8.5%)	9 (9%)	
LH / FSH	51 (30.9%)	35 (35%)	
PRL	17 (10.3%)	5 (5%)	
0 CELL	44 (26.7%)	26 (26%)	
TSH	1 (0.6%)	1 (1%)	
PRL + GH	6 (3.6%)	5 (5%)	
PLURI	5 (3%)	2 (2%)	
APOPLECTIC	3 (1.8%)	2 (2%)	

The mean displacement of the right ICA in group Non-Inv was 12.364 mm (SD ± 2.706, p = 0.064) respectively 13.493 mm (SD: 2.596, p = 0.038) of the left ICA. The mean displacement of the right ICA in the group Inv was 13.040 mm (SD ± 3.081, p = 0.064) respectively 14.209 (SD: 2.853, p = 0.038) of the left ICA.
The revised Knosp Grading (2) in group Non-Inv showed: Grade 0: 62 (37.6%), Grade 1: 38 (23%), Grade 2: 32 (19.4%), Grade 3A: 25 (15.2%), Grade 3B: 4 (2.4%) and Grade 4: 4 (2.4%). In group Inv: Grade 0: 23 (23%), Grade 1: 17 (17%), Grade 2: 14 (14%), Grade 3A: 22 (22%), Grade 3B: 5 (5%) and Grade 4: 19 (19%); (p = < 0.001). Particularly Grade 4 pituitary adenomas were found significantly more often in group Inv (19%) than in group Non-Inv (2.4%, p = < 0.001). In contrast, the percentages of grades 0,1 and 2 were non-significantly higher than in group Non-Inv. (**Figure 10**)

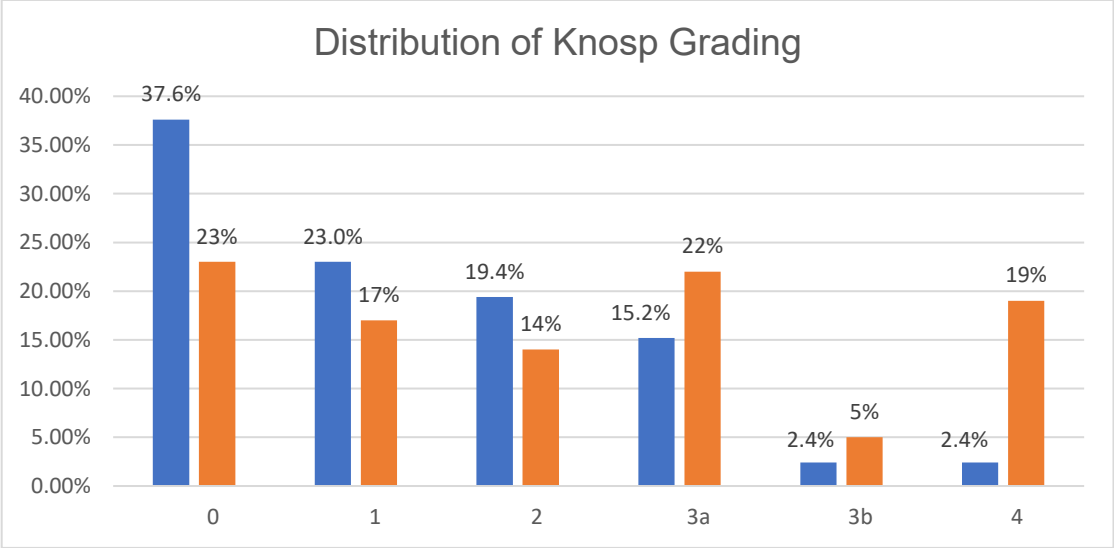

Figure 10: Bar chart with the distribution of Knosp grading for the study groups Non-Inv (blue) and Inv (orange).

The Hardy Grading (58,59) in group Non-Inv yielded: Grade 0: 48 (29.1%), Grade A: 70 (42.4%), Grade B: 42 (25.5%), Grade C: 5 (3%). In group Inv: Grade 0: 26 (26%), grade A: 35 (35%), Grade B: 35 (35%), Group C: 3 (3%) and Group D: 1: 1(1%) were found (p = 0.322).

The histopathological subtypes within group Non-Inv showed: ACTH: 24 (14.5%), GH: 14 (8.5%), LH / FSH: 51 (30.9%), PRL 17 (10.3%), null cell: 44 (26.7%), TSH: 1 (0.6%), PRL + GH: 6 (3.6%), plurihormonal: 5 (3%) and apoplectic: 3 (1.8%).

In group Inv the data showed: ACTH: 15 (15%), GH: 9 (9%), LH / FSH: 35 (35%), PRL 5 (5%), null cell: 26 (26%), TSH 1 (1%), PRL + GH 5 (5%), plurihormonal 2 (2%) and apoplectic 2 (2%) (p=0.925).

In case pituitary adenoma consistency, firm and calcified adenomas were detected significantly more often in group Inv (p = 0.005). In contrast, the percentage of cystic, soft and average adenomas was higher in group Non-Inv. **(Table 2)**

	NON-INV	**INV**	**P-VALUE**
NUMBER (N=260)	161	99	
CONSISTENCY			**0.005**
CYSTIC	5 (3.1%)	0	
SOFT	29 (18%)	12 (12.1%)	
AVERAGE	107 (66.5%)	58 (58.6%)	
FIRM	20 (12.4%)	28 (28.3%)	
CALCIFIED	0	1 (1%)	

Table 2: Adenoma consistency characteristics of patients with histopathological confirmed pituitary adenoma.

An intraoperative total resection was achieved in 72.4% in group Non-Inv. In contrast, a total resection was achieved in 28% in group Inv. Furthermore, a subtotal resection was achieved in 64% in group Inv, while in group Non-Inv a subtotal resection was possible in 23.3% of cases (p = < 0.001). **(Table 3)**

	NON-INV	**INV**	**P-VALUE**
NUMBER (N=263)	163	100	
DEGREE OF RESECTION			**< 0.001**
PARTIAL	7 (4.3%)	8 (8%)	
SUBTOTAL	38 (23.3%)	64 (64%)	
TOTAL	118 (72.4%)	28 (28%)	

Table 3: Resection rates of patients with histopathological confirmed pituitary adenoma.

The evaluation of postoperative gross total resection/endocrine remission showed that 21.9% of group Inv met these criteria. In contrast, 51.6% of group Non-Inv achieved gross total resection/endocrine remission (p = < 0.001). **(Table 4)**

	NON-INV	INV	P-VALUE
NUMBER (N=253)	157	96	
REMISSION			**< 0.001**
NO	76 (48.4%)	75 (78.1%)	
YES	81 (51.6%)	21 (21.9%)	

Table 4: Remission rates of patients with histopathological confirmed pituitary adenoma.

3.2 Multivariate regression model - Macroadenomas

To assess the effect on endoscopically observed invasion while controlling for potential confounding factors, we employed a multiple binomial regression model. For this model, we tested pituitary adenomas that were larger than 10 mm in diameter (macroadenomas). The binomial regression model reached a significance level of X^2 (7) = 24.063; p = < 0.001 overall. This model showed that macroadenomas which have a volume above 1 cm³ (OR: 4.627, 95% CI: 1.476–14.498, p = 0.009) are independently associated with invasion into the cavernous sinus. In addition, it can be established that the odds ratio (3.275, 95% CI: 1.649–6.503) for adenomas with a fibrous consistency is significantly (p = < 0.001) higher as for adenomas with a soft consistency. The remaining factors and the other dichotomous volume groups tested in the model did not reach a level of significance.

	ODDS RATIO FOR INVASION (95% CI; P-VALUE)
VOLUME (< 1 CM ³, > 1 CM³)	**4.627 (1.476–14.498, 0.009)**
CONSISTENCY OF THE ADENOMA (SOFT / FIBROUS)	**3.275 (1.649–6.503, < 0.001)**
FUNCTIONAL STATUS (NON-FUNCTIONING / FUNCTIONING)	2.006 (0.966–4.166, 0.062)
POSTERIOR CLINOID PROCESS	0.057 (0.480–1.022, 0.057)
AGE (< 60, > 60)	1.001 (0.553–1.811, 0.997)
DISPLACEMENT OF THE LEFT ICA (NO / YES)	2.618 (0.153–44.928, 0.507)
DISPLACEMENT OF THE RIGHT ICA (NO / YES)	2.605 (0.152–44.689, 0.509)

Table 5: A multivariate logistic regression was used to control for potential confounding factors and to determine the effect of volume > 1cm³, consistency fibrous, functional status, posterior clinoid process visible, age > 60, displacement of the left and right ICA on endoscopically observed invasion into the CS.

3.3 Multivariate regression model - Non-functioning adenomas

For the multivariate regression model, only non-functioning adenomas were tested. To determine the effect on endoscopically observed invasion we used a binomial multivariate regression model. The binomial regression model reached overall a significance level of X^2 (6) = 19.331; p = 0.004. This model showed that non-functioning adenomas which have a volume above 1.6 cm^3 (OR: 4.091, 95%: CI 1.310–12.778, p = 0.015) are independently associated with invasion into the cavernous sinus. Furthermore, as established in the previous regression model for macroadenomas, the odds ratio (2.710, 95% CI: 1.250–5.875) for invasion into the cavernous sinus for fibrous adenomas is significantly (p = 0.012) higher as for adenomas with a soft consistency. The remaining factors and the other dichotomous volume groups tested in the model did not reach a level of significance.

	ODDS RATIO FOR INVASION (95% CI; P-VALUE)
VOLUME (< 1.6 CM ^{3}, > 1.6 CM³)	**4.091 (1.310–12.778, 0.015)**
CONSISTENCY OF THE ADENOMA (SOFT / FIBROUS)	**2.710 (1.250–5.875, 0.012)**
POSTERIOR CLINOID PROCESS (NO / YES)	0.471 (0.208–1.066, 0.071)
AGE (< 60, > 60)	0.918 (0.482–1.748, 0.794)
DISPLACEMENT OF THE LEFT ICA (NO / YES)	2.253 (0.128–39.511, 0.578)
DISPLACEMENT OF THE RIGHT ICA (NO / YES)	2.553 (0.146–44.574, 0.521)

Table 6: A multivariate logistic regression was used to control for potential confounding factors and to determine the effect of volume > 1,6cm³, consistency fibrous, posterior clinoid process visible, age > 60, displacement of the left and right ICA on endoscopically observed invasion into the CS.

3.4 Moderation analysis

A moderation analysis with the PROCESS macro for SPSS by Hayes (2018) (66) was chosen to determine whether the volume and the interaction of invasion significantly predicts the displacement of the left cavernous ICA.

The overall model showed significant results: $R^2 = 10.41$, F (13.4997), p = < 0.001. The model showed that the increase of 1 Unit, e.g. 1 cm^3 of non-invasive adenomas increases the displacement for the left ICA about 0.2153 mm (p = < 0.001) while invasive adenomas displace the ICA about 0.0311 mm for every cm^3 increase in volume. As a result, invasion significantly moderates (-0.1842 mm per unit of 1 cm^3) the effect between displacement and volume. However, it should be noted that the overall displacement of invasive adenomas is consistently higher (p = < 0.001), but as described previously, with each 1 cm^3 increase of volume, invasive adenomas displace the ICA approximately 0,1842 mm less than non-invasive adenomas.

	CHANGE OF DISPLACEMENT IN MM	P-VALUE
INCREASE IN VOLUME BY 1CM3	0.2153	< 0.001
MODERATION INVASION	-0.1842	0.004
CONSTANT INCREASE OF DISPLACEMENT WHEN INVASIVE	1.2935	< 0.001

Table 7: A moderation analysis with the PROCESS macro by Hayes (2018) was used to determine the interaction between the displacement of the left ICA in mm, invasion and volume of the pituitary adenoma in cm^3.

The same statistical analysis was used for the right cavernous ICA but no significant level for the moderation variable “invasion” was reached.

4. Discussion

Overall, seven variables of baseline-characteristics differed significantly between invasive and non-invasive pituitary adenomas. These characteristics were size, volume, displacement of the left ICA, revised Knosp Grading (2), consistency of the pituitary adenoma, degree of resection and gross total resection/endocrine remission.

Parasellar Tumor Extension - Revised Knosp Grading

A systematic review by Dhandapani et al. (2016) searched the MEDLINE database (1993–2015) to investigate studies on radiological criteria for invasion into the CS, acknowledging that Knosp Grade 3 and Grade 4 are the most reliable indicators for invasion into the CS (67).

The results of the applied revised Knosp Grading showed that grades 3A (22% vs. 15.2%, superior compartment), 3B (5% vs. 2.4%, inferior compartment) (2) and 4 (superior, inferior and lateral compartment) (37) are more likely to invade the CS. Particularly Grade 4 pituitary adenomas were found significantly more often in group Inv (19%) than in group Non-Inv (2.4%). Consequently, the categorization into low-grade (0,1,2) and high-grade (3A,3B,4) in relation to invasion appears to be confirmed (67).

It is also noteworthy, that in group Inv, invasion into the superior compartment was significantly more prevalent than invasion into the inferior compartment of the CS (22% vs. 5%, $p = < 0.001$).

Interestingly, the Non-Inv group showed also 15.2% of grade 3A adenomas without signs of invasion, highlighting the need for careful differentiation between displacement and true invasion into the superior compartment of the CS (1,2).

In the pioneer work from Micko et al. (2015), the percentage of grades 3B adenomas which showed clear signs of invasion into the inferior compartment was much higher compared to the percentage of grades 3A adenomas with invasion into the superior compartment (70.6% vs. 26.5%).

In general, parasellar invasion of pituitary adenomas into the CS is a significant prognostic element for the degree of resection in non-functioning pituitary adenomas and for decrease in remission rates in functioning pituitary adenomas (1,2). This is consistent with our data, where regardless of functional status, postoperative gross total resection/endocrine remission rates fall from 51.6% to 21.9% and total resection rates of pituitary adenomas fall from 72.4% to 28% when invasion into the CS was present.

Tumor size and Volume

The size of pituitary adenomas can be determined either by categorizing them according to their maximum diameter as seen on MRI-scans, or by measuring their volume using a variety of different methods (68). Maximum diameter is a simpler method for measurement, but inaccurate because of the general cubic relationship between diameter and tumor volume (68). Particularly when clinically accurate statements have to be made, measuring the volume is the preferred method (68).
In our work, the median volume (measured in cm^3) in the group Non-Inv was 2.5 cm^3 (IQR: 1.2–6.7) while the median volume in the group Inv was 7.3 cm^3 (IQR: 2.8–13.3). Therefore, it can be concluded that pituitary adenomas invading the CS tend to have a larger median volume ($p = < 0.001$).
Kawamoto et al. (1995) could also show that the volume of non-functioning adenomas demonstrating invasion into the CS was significantly higher than for non-functioning adenomas with no observed invasion (69).
Aislyn Di Risio et al. (2022) analyzed 143 patients with non-functioning macroadenomas and their relationship with degree of resection (70). They were able to determine that tumor volume is a significant factor for the prediction of degree of resection (70). Furthermore, their multivariate logistic regression model showed, that a smaller volume is an independent predictor for higher resection rates (70).
In contrast, our multivariate logistic regression model showed that that non-functioning adenomas which have a volume greater than 1.6 cm^3 (OR: 4.091, 95% CI: 1.310–12.778, $p = 0.015$) are independently associated with invasion into the CS. Regardless of functional status, the odds ratio for invasion into the CS of

macroadenomas is 4.627 (95% CI: 1.476–14.498, p = 0.009) for pituitary adenomas with a volume greater than 1 cm³.

In a literature review, Esposito et al. (2019) assessed indications for non-functioning pituitary adenomas (22). Indications and strategies for asymptomatic non-functioning pituitary adenomas vary considerably from one another (22).

A systematic review from the congress of neurological surgeons stated a level 3 recommendation for surgical resection of symptomatic patients with non-functioning pituitary adenomas (71). If there are no clinical signs, such as headache in the frontal and occipital regions, bitemporal visual defects, hormone deficiencies, hyperprolactinemia or diabetes insipidus are present, individualized surveillance should be considered (22). Our data suggest that non-functioning pituitary adenomas with a volume exceeding 1.6 cm³ are more likely to grow invasively into the CS and therefore surgery should be considered.

Figure 11: Example of a non-functioning adenoma, Coronal T1-weighted contrast-enhanced MRI-scan. Volume 1.2 cm³

Figure 11 illustrates an example of a non-functioning pituitary adenoma with a volume of 1.2 cm³. At the time of the MRI-scan, the patient had no clinical symptoms like headache, visual defects, hormone deficiencies and hyperprolactinemia. Furthermore, no radiological parasellar invasion into the CS was present.

Displacement vs. Invasion

With regard to parasellar growth of pituitary adenomas, a distinction should be made between pure displacement and invasion (1). In the event of pure displacement, the intact medial wall without signs of infiltration is only displaced by the pressure of the parasellar growing pituitary adenoma mass (72). However, if adenoma tissue is visible intraoperatively within the CS space, a medial wall that is intraoperatively no longer intact or detectable, structures of the CS or the adventitia of the ICA are visible intraoperatively, pituitary adenomas are considered invasive (2).
Regarding the topic of displacement of the ICA vs. invasion, Cottier et al. (2000) demonstrated, that the lateral displacement of the cavernous ICA was not a reliable sign for invasion (73).
To determine whether there is an association between volume and displacement of the cavernous ICA, or rather differences in growth patterns in our two study groups in relation to the displacement of the ICA, we generated a moderated regression model for the left and right ICA. The moderating factor was invasion into the CS. Interestingly, the model was not significant for the right ICA. However, for the left ICA the model demonstrated that invasion moderated an effect between volume and displacement of the left ICA significantly ($p = 0.004$). This model provides a potential explanation for the tendency of invasive adenomas regarding their infiltrative growth patterns, while non-invasive adenomas tend to displace the parasellar structures (1). However, invasive adenomas generally have a higher volume and therefore, on average, still show a higher displacement of the left ICA (14.21 mm vs. 13.50 mm, $p = 0.038$).

Tumor Consistency

Rutkowski et al. (2021) found that 59.3% of cases with a firm or calcified consistency demonstrated an invasion into the CS (63). Micko et al. (2020) similarly found that 52% of cases with Knosp Grade 4 and invasion into the CS demonstrated a fibrous consistency (1). Rutkowski et al. (2021) tried to explain this phenomenon of the presence of intrinsic differences in adenomas with potential correlation with their immunological microenvironment and general increased collagen content (63).

As can be seen in both multivariate regression models, adenoma consistency is significantly independently related to invasion into the CS ($p = < 0.001$, $p = 0.012$). This information, whether an adenoma has a fibrous consistency, could be very valuable preoperatively but a literature review from Thotakura et al. (2017) showed, that it is not possible to reliable assess the consistency of pituitary adenomas preoperatively on MRI-scans (74). However, in a recent work by Yildirim et al. (2024), biomarkers for the consistency of macroadenomas could be predicted by using multi-dynamic-multi-echo based relaxometry (75).

Limitations

This thesis has several limitations due to the retrospective character of the study. First, the total number of Grade 3B and Grade 4 adenomas was low with 31 cases in the context of the assessment. Furthermore, the number of different surgeons was relatively high and consistency slightly dependent on their subjective opinion. Acquisition of data was performed by four different persons, which could increase the risk of potential bias.

5. Conclusion

In summary, a correlation has been demonstrated between the size, volume, and consistency of the adenoma and its invasion into the CS.

In particular, a fibrous consistency of the pituitary adenomas showed a strong independent association with invasiveness into the CS. Moreover, it could be hypothesized that non-functioning pituitary adenomas with a volume greatest than 1.6 cm^3 are independently associated with invasion into the CS.

Furthermore, pituitary adenomas Knosp Grade 3A can either displace or invade the superior compartment while adenomas classified as Knosp Grade 4 demonstrated with higher probability an invasion into the superior, inferior and lateral compartments of the CS.

In addition, a moderated regression model was used to analyze the differences in growth patterns in relation to the displacement of the ICA, in the realization that further research in this topic will be necessary.

The findings of this thesis indicate that specific preoperative parameters can predict the invasiveness of a pituitary adenoma. These factors may facilitate improved patient counselling and contribute to the development of a multimodal treatment strategy, incorporating surgical intervention, medical therapy, and radiosurgery.

References

1. Micko A, Oberndorfer J, Weninger WJ, Vila G, Höftberger R, Wolfsberger S, et al. Challenging Knosp high-grade pituitary adenomas. J Neurosurg. 2020 Jun;132(6):1739–46.

2. Micko ASG, Wöhrer A, Wolfsberger S, Knosp E. Invasion of the cavernous sinus space in pituitary adenomas: endoscopic verification and its correlation with an MRI-based classification. J Neurosurg. 2015 Apr;122(4):803–11.

3. Gijn DR van. Oxford handbook of head and neck anatomy. First edition. Standring S, Eccles S, editors. Oxford, United Kingdom: Oxford University Press; 2022.

4. Amar AP, Weiss MH. Pituitary anatomy and physiology. Neurosurg Clin N Am. 2003 Jan;14(1):11–23.

5. Melmed S, Kaiser UB, Lopes MB, Bertherat J, Syro LV, Raverot G, et al. Clinical Biology of the Pituitary Adenoma. Endocr Rev. 2022 Nov 25;43(6):1003–37.

6. Hong GK, Payne SC, Jane JA. Anatomy, Physiology, and Laboratory Evaluation of the Pituitary Gland. Otolaryngol Clin North Am. 2016 Feb;49(1):21–32.

7. Waldeyer A, Anderhuber F, Pera F, Streicher J, editors. Waldeyer - Anatomie des Menschen: Lehrbuch und Atlas in einem Band ; [44 Tabellen]. 19., vollst. überarb. und aktualisierte Auflage. Berlin: de Gruyter; 2012. 1176 p. (De Gruyter Studium).

8. Kahle W, Frotscher M, Schmitz F, Spitzer G. Nervensystem und Sinnesorgane. 12., aktualisierte Auflage. Stuttgart New York: Georg Thieme Verlag; 2018. 439 p. (Taschenatlas Anatomie).

9. Lüllmann-Rauch R, Asan E. Taschenlehrbuch Histologie. 6., vollständig überarbeitete Auflage. Stuttgart New York: George Thieme Verlag; 2019. 781 p.

10. Asmaro K, Zhang M, Rodrigues AJ, Mohyeldin A, Vigo V, Nernekli K, et al. Cytodifferentiation of pituitary tumors influences pathogenesis and cavernous sinus invasion. J Neurosurg. 2023 Apr 1;1–9.

11. Balcerzak A, Tubbs RS, Zielinska N, Olewnik Ł. Clinical analysis of cavernous sinus anatomy, pathologies, diagnostics, surgical management and complications – Comprehensive review. Ann Anat - Anat Anz. 2023 Jan;245:152004.

12. Trouillas J, Jaffrain-Rea ML, Vasiljevic A, Raverot G, Roncaroli F, Villa C. How to Classify Pituitary Neuroendocrine Tumors (PitNET)s in 2020. Cancers. 2020 Feb 22;12(2):514.

13. Lopes MBS. The 2017 World Health Organization classification of tumors of the pituitary gland: a summary. Acta Neuropathol (Berl). 2017 Oct;134(4):521–35.

14. Melmed S. Pituitary-Tumor Endocrinopathies. Longo DL, editor. N Engl J Med. 2020 Mar 5;382(10):937–50.

15. Klinke R, Pape HC, Kurtz A, Silbernagl S, editors. Physiologie [Internet]. 6th ed. Stuttgart: Georg Thieme Verlag; 2010 [cited 2024 Aug 15]. Available from: https://eref.thieme.de/10.1055/b-002-46974

16. Cironi KA, Decater T, Iwanaga J, Dumont AS, Tubbs RS. Arterial Supply to the Pituitary Gland: A Comprehensive Review. World Neurosurg. 2020 Oct;142:206–11.

17. Mitsuhashi Y, Hayasaki K, Kawakami T, Nagata T, Kaneshiro Y, Umaba R, et al. Dural Venous System in the Cavernous Sinus: A Literature Review and Embryological, Functional, and Endovascular Clinical Considerations. Neurol Med Chir (Tokyo). 2016;56(6):326–39.

18. Raverot G, Burman P, McCormack A, Heaney A, Petersenn S, Popovic V, et al. European Society of Endocrinology Clinical Practice Guidelines for the management of aggressive pituitary tumours and carcinomas. Eur J Endocrinol. 2018 Jan;178(1):G1–24.

19. Asa SL, Casar-Borota O, Chanson P, Delgrange E, Earls P, Ezzat S, et al. From pituitary adenoma to pituitary neuroendocrine tumor (PitNET): an International Pituitary Pathology Club proposal. Endocr Relat Cancer. 2017 Apr;24(4):C5–8.

20. Ho KKY, Fleseriu M, Wass J, Van Der Lely A, Barkan A, Giustina A, et al. A tale of pituitary adenomas: to NET or not to NET: Pituitary Society position statement. Pituitary. 2019 Dec;22(6):569–73.

21. Melmed S, Casanueva FF, Hoffman AR, Kleinberg DL, Montori VM, Schlechte JA, et al. Diagnosis and Treatment of Hyperprolactinemia: An Endocrine Society Clinical Practice Guideline. J Clin Endocrinol Metab. 2011 Feb;96(2):273–88.

22. Esposito D, Olsson DS, Ragnarsson O, Buchfelder M, Skoglund T, Johannsson G. Non-functioning pituitary adenomas: indications for pituitary surgery and post-surgical management. Pituitary. 2019 Aug;22(4):422–34.

23. Hong JW, Lee MK, Kim SH, Lee EJ. Discrimination of prolactinoma from hyperprolactinemic non-functioning adenoma. Endocrine. 2010 Feb;37(1):140–7.

24. Caron P, Brue T, Raverot G, Tabarin A, Cailleux A, Delemer B, et al. Signs and symptoms of acromegaly at diagnosis: the physician’s and the patient’s perspectives in the ACRO-POLIS study. Endocrine. 2019 Jan;63(1):120–9.

25. Ershadinia N, Tritos NA. Diagnosis and Treatment of Acromegaly: An Update. Mayo Clin Proc. 2022 Feb;97(2):333–46.

26. Nieman LK. Diagnosis of Cushing's Syndrome in the Modern Era. Endocrinol Metab Clin North Am. 2018 Jun;47(2):259–73.

27. Beck-Peccoz P, Persani L, Mannavola D, Campi I. TSH-secreting adenomas. Best Pract Res Clin Endocrinol Metab. 2009 Oct;23(5):597–606.

28. Drummond J, Roncaroli F, Grossman AB, Korbonits M. Clinical and Pathological Aspects of Silent Pituitary Adenomas. J Clin Endocrinol Metab. 2019 Jul 1;104(7):2473–89.

29. Chen L, White WL, Spetzler RF, Xu B. A prospective study of nonfunctioning pituitary adenomas: presentation, management, and clinical outcome. J Neurooncol. 2011 Mar;102(1):129–38.

30. Bergland RM, Ray BS, Torack RM. Anatomical Variations in the Pituitary Gland and Adjacent Structures in 225 Human Autopsy Cases. J Neurosurg. 1968 Feb;28(2):93–9.

31. Rhoton AL. The Cavernous Sinus, the Cavernous Venous Plexus, and the Carotid Collar. Neurosurgery. 2002 Oct 1;51(suppl_4):S1-375-S1-410.

32. Fernandez-Miranda JC, Zwagerman NT, Abhinav K, Lieber S, Wang EW, Snyderman CH, et al. Cavernous sinus compartments from the endoscopic endonasal approach: anatomical considerations and surgical relevance to adenoma surgery. J Neurosurg. 2018 Aug;129(2):430–41.

33. Truong HQ, Lieber S, Najera E, Alves-Belo JT, Gardner PA, Fernandez-Miranda JC. The medial wall of the cavernous sinus. Part 1: Surgical anatomy, ligaments, and surgical technique for its mobilization and/or resection. J Neurosurg. 2019 Jul;131(1):122–30.

34. Trepel M. Neuroanatomie: Struktur und Funktion. 7. Auflage. München: Elsevier; 2017. 419 p.

35. Vijaywargiya M, Deopujari R, Athavale SA. Anatomical study of petrous and cavernous parts of internal carotid artery. Anat Cell Biol. 2017;50(3):163.

36. Bouthillier A, Van Loveren HR, Keller JT. Segments of the Internal Carotid Artery: A New Classification. Neurosurgery. 1996 Mar 1;38(3):425–33.

37. Xu Y, Asmaro K, Lee CK, Vigo V, Mohyeldin A, Nunez MA, et al. Lateral compartment of the cavernous sinus from the endoscopic endonasal approach: anatomical considerations and surgical relevance to adenoma surgery. J Neurosurg. 2024 Aug 1;1–13.

38. Xu Y, Mohyeldin A, Asmaro KP, Nunez MA, Doniz-Gonzalez A, Vigo V, et al. Intracranial Breakthrough Through Cavernous Sinus Compartments:

Anatomic Study and Implications for Pituitary Adenoma Surgery. Oper Neurosurg. 2022 Aug;23(2):115–24.

39. Yasuda A, Campero A, Martins C, Rhoton AL, De Oliveira E, Ribas GC. Microsurgical Anatomy and Approaches to the Cavernous Sinus: Oper Neurosurg. 2005 Jan;56:4–27.

40. Dolenc VV. Anatomy and Surgery of the Cavernous Sinus. Vienna: Springer Vienna; 1989.

41. Hendricks BK, Benet A, Lawrence PM, Benner D, Preul MC, Lawton MT. Anatomical Triangles for Use in Skull Base Surgery: A Comprehensive Review. World Neurosurg. 2022 Aug;164:79–92.

42. Knosp E, Steiner E, Kitz K, Matula C. Pituitary Adenomas with Invasion of the Cavernous Sinus Space: A Magnetic Resonance Imaging Classification Compared with Surgical Findings. Neurosurgery. 1993 Oct;33(4):610–8.

43. Iaconetta G, Fusco M, Samii M. The sphenopetroclival venous gulf: a microanatomical study. J Neurosurg. 2003 Aug;99(2):366–75.

44. Iaconetta G, Fusco M, Cavallo LM, Cappabianca P, Samii M, Tschabitscher M. The Abducens Nerve: Microanatomic and Endoscopic Study. Oper Neurosurg. 2007 Sep;61(3):7–14.

45. Grewal SS, Kurbanov A, Anaizi A, Keller JT, Theodosopoulos PV, Zimmer LA. Endoscopic endonasal approach to the maxillary strut: Anatomical review and case series. The Laryngoscope. 2014 Aug;124(8):1739–43.

46. Salaud C, Decante C, Ploteau S, Hamel A. Implication of the inferolateral trunk of the cavernous internal CAROTID artery in cranial nerve blood supply: Anatomical study and review of the literature. Ann Anat - Anat Anz. 2019 Nov;226:23–8.

47. Funaki T, Matsushima T, Peris-Celda M, Valentine RJ, Joo W, Rhoton AL. Focal Transnasal Approach to the Upper, Middle, and Lower Clivus. Oper Neurosurg. 2013 Dec;73:ons155–91.

48. Cheng Y, Chen Y, Zhou Z, Zhu J, Feng Y, Zhao G. Anatomical Study of Posterior Clinoid Process (PCP) and Its Clinical Meanings. J Craniofac Surg. 2015 Mar;26(2):537–40.

49. Xu Y, Lee CK, Rychen J, Arifianto MR, Nunez MA, Cohen-Gadol AA, et al. Extended transcavernous posterior clinoidectomy in endoscopic endonasal surgery. J Neurosurg. 2024 Oct 1;1–11.

50. Serioli S, Plou P, Leonel LCPC, Graepel S, Buffoli B, Rezzani R, et al. The “candy wrapper” of the pituitary gland: a road map to the parasellar ligaments and the medial wall of the cavernous sinus. Acta Neurochir (Wien) [Internet]. 2023 Aug 18 [cited 2023 Oct 2]; Available from: https://link.springer.com/10.1007/s00701-023-05736-x

51. Salma A, Baidya N, Wendt B, Aguila F, Sammet S, Ammirati M. Qualitative and Quantitative Radio-Anatomical Variation of the Posterior Clinoid Process. Skull Base. 2011 Nov;21(06):373–8.

52. Gonçalves MB, De Oliveira JG, Williams HA, Alvarenga RMP, Landeiro JA. Cavernous sinus medial wall: dural or fibrous layer? Systematic review of the literature. Neurosurg Rev. 2012 Apr;35(2):147–54.

53. Yokoyama S, Moroki K, Imamura S. Are Nonfunctioning Pituitary Adenomas Extending into the Cavernous Sinus Aggressive and/or Invasive? 2001;49(4).

54. Yasuda A, Campero A, Martins C, Rhoton AL, Ribas GC. The Medial Wall of the Cavernous Sinus: Microsurgical Anatomy. Neurosurgery. 2004 Jul;55(1):179–90.

55. Micko A, Hosmann A, Marik W, Bartsch S, Weber M, Knosp E, et al. Optimizing MR imaging for intraoperative image guidance in sellar pathologies. Pituitary. 2020 Jun;23(3):266–72.

56. Mert A, Micko A, Donat M, Maringer M, Buehler K, Sutherland GR, et al. An Advanced Navigation Protocol for Endoscopic Transsphenoidal Surgery. World Neurosurg. 2014 Dec;82(6):S95–105.

57. Vieira JO, Cukiert A, Liberman B. Evaluation of magnetic resonance imaging criteria for cavernous sinus invasion in patients with pituitary adenomas: logistic regression analysis and correlation with surgical findings. Surg Neurol. 2006 Feb;65(2):130–5.

58. Hardy J, Wigser SM. Trans-sphenoidal Surgery of Pituitary Fossa Tumors with Televised Radiofluoroscopic Control. J Neurosurg. 1965 Dec;23(6):612–9.

59. Hardy J, Vezina JL. Transsphenoidal neurosurgery of intracranial neoplasm. Adv Neurol. 1976;15:261–73.

60. Organisation mondiale de la santé, Centre international de recherche sur le cancer, editors. WHO classification of tumours of endocrine organs. 4th ed. Lyon: International agency for research on cancer; 2017. (World health organization classification of tumours).

61. Thapar K, Kovacs K, Scheithauer BW, Stefaneanu L, Horvath E, Peter J. P, et al. Proliferative Activity and Invasiveness among Pituitary Adenomas and Carcinomas: An Analysis Using the MIB-1 Antibody. Neurosurgery. 1996 Jan;38(1):99–107.

62. Bahuleyan B, Raghuram L, Rajshekhar V, Chacko AG. To assess the ability of MRI to predict consistency of pituitary macroadenomas. Br J Neurosurg. 2006 Jan;20(5):324–6.

63. Rutkowski MJ, Chang KE, Cardinal T, Du R, Tafreshi AR, Donoho DA, et al. Development and clinical validation of a grading system for pituitary adenoma consistency. J Neurosurg. 2021 Jun;134(6):1800–7.

64. Cappabianca P, Cavallo LM, Colao A, De Divitiis E. Surgical complications associated with the endoscopic endonasal transsphenoidal approach for pituitary adenomas. J Neurosurg. 2002 Aug;97(2):293–8.

65. Micko ASG, Wöhrer A, Höftberger R, Vila G, Marosi C, Knosp E, et al. MGMT and MSH6 immunoexpression for functioning pituitary macroadenomas. Pituitary. 2017 Dec;20(6):643–53.

66. Hayes AF, Little TD. Introduction to mediation, moderation, and conditional process analysis: a regression-based approach. Second edition. New York London: The Guilford Press; 2018. 692 p. (Methodology in the social sciences).

67. Dhandapani S, Singh H, Negm HM, Cohen S, Anand VK, Schwartz TH. Cavernous Sinus Invasion in Pituitary Adenomas: Systematic Review and Pooled Data Meta-Analysis of Radiologic Criteria and Comparison of Endoscopic and Microscopic Surgery. World Neurosurg. 2016 Dec;96:36–46.

68. Egger J, Kapur T, Nimsky C, Kikinis R. Pituitary Adenoma Volumetry with 3D Slicer. Muñoz-Barrutia A, editor. PLoS ONE. 2012 Dec 11;7(12):e51788.

69. Kawamoto H, Uozumi T, Kawamoto K, Arita K, Yano T, Hirohata T. Analysis of the growth rate and cavernous sinus invasion of pituitary adenomas. Acta Neurochir (Wien). 1995 Mar;136(1–2):37–43.

70. DiRisio AC, Feng R, Shuman WH, Platt S, Price G, Dullea JT, et al. The Knosp Criteria Revisited: 3-Dimensional Volumetric Analysis as a Predictive Tool for Extent of Resection in Complex Endoscopic Pituitary Surgery. Neurosurgery. 2023 Jan;92(1):179–85.

71. Lucas JW, Bodach ME, Tumialan LM, Oyesiku NM, Patil CG, Litvack Z, et al. Congress of Neurological Surgeons Systematic Review and Evidence-Based Guideline on Primary Management of Patients With Nonfunctioning Pituitary Adenomas. Neurosurgery. 2016 Oct;79(4):E533–5.

72. Ahmadi J, North C, Segall H, Zee C, Weiss M. Cavernous sinus invasion by pituitary adenomas. 1986;

73. Cottier JP, Destrieux C, Brunereau L, Bertrand P, Moreau L, Jan M, et al. Cavernous Sinus Invasion by Pituitary Adenoma: MR Imaging. Radiology. 2000 May;215(2):463–9.

74. Thotakura AK, Patibandla MR, Panigrahi MK, Mahadevan A. Is it really possible to predict the consistency of a pituitary adenoma preoperatively? Neurochirurgie. 2017 Dec;63(6):453–7.

75. Yildirim MS, Schmidbauer VU, Micko A, Lechner L, Weber M, Furtner J, et al. Multi-Dynamic-Multi-Echo-based MRI for the Pre-Surgical Determination of Sellar Tumor Consistency: a Quantitative Approach for Predicting Lesion Resectability. Clin Neuroradiol. 2024 Sep;34(3):663–73.

In this work, AI-based tools were used solely to optimize the language or wording in accordance with the applicable standards for good scientific practice of the Medical University of Graz.

The following tools were used to optimize the language of the text:

1. DeepL Write, DeepL SE, https://www.deepl.com/de/write
2. ChatGPT 4.0, OpenAI, https://chatgpt.com